Chapter 1. 銀河宇宙物理の基礎

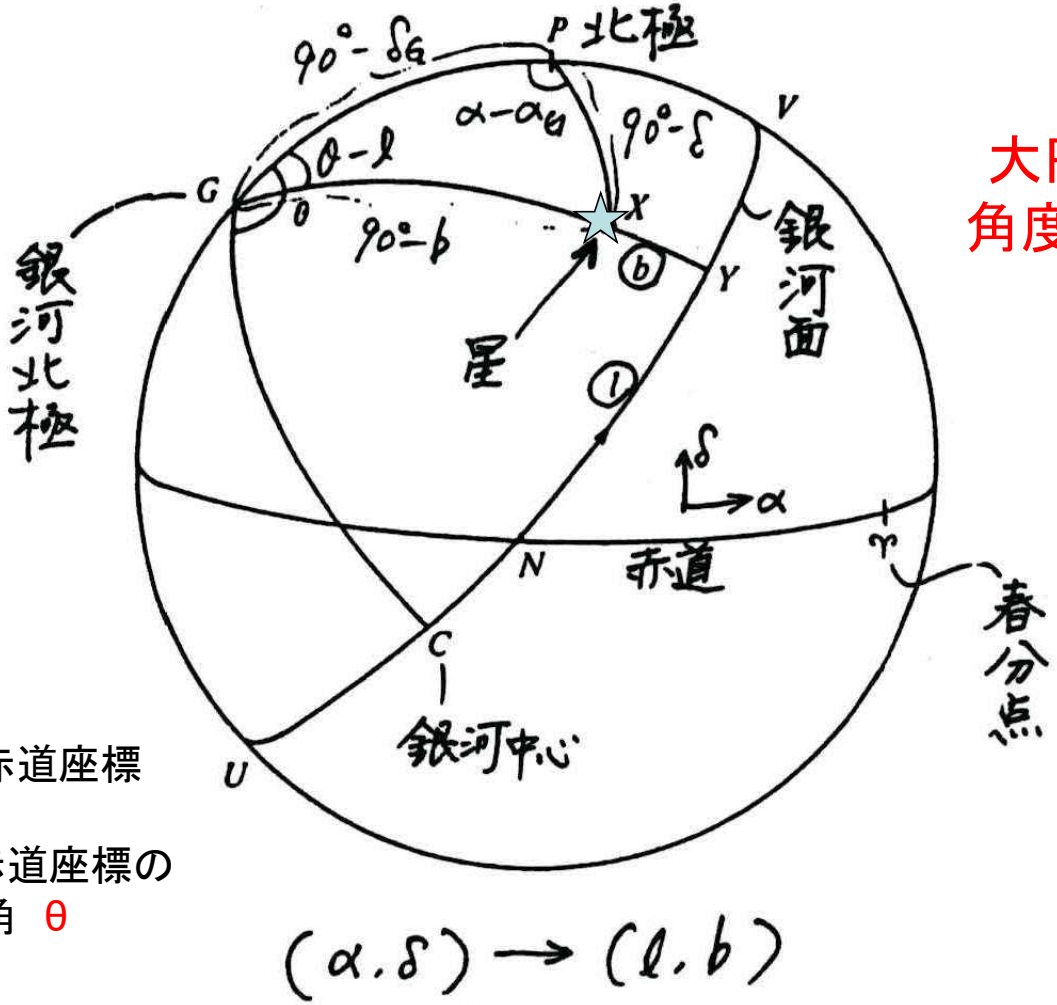

大円上で
角度を取る

・銀河北極の赤道座標
（α_G, δ_G ）
・銀河中心と赤道座標の
北極のなす角　θ

赤道座標　　銀河座標

Astrometry Satellites

	ヒッパルコス衛星 1989~1993	ガイア衛星 2013~2021～
	Hipparcos	**Gaia**
Magnitude limit	12 mag	20 mag
Completeness	7.3 – 9.0 mag	20 mag
Bright limit	0 mag	6 mag
Number of objects	120,000	26 million to V = 15 250 million to V = 18 1000 million to V = 20
Effective distance	1 kpc	50 kpc
Quasars	1 (3C 273)	500,000
Galaxies	None	1,000,000
Accuracy	1 milliarcsec	7 μarcsec at V = 10 10 – 25 μarcsec at V = 15 300 μarcsec at V = 20
Photometry	2-colour (B and V)	Low-res. spectra to V = 20
Radial velocity	None	15 km s^{-1} to V = 17
Observing	Pre-selected	Complete and unbiased

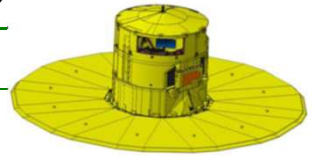

DR3 (2022 June)
1.46 billion stars
G<21 mag

https://www.cosmos.esa.int/web/gaia/dr3

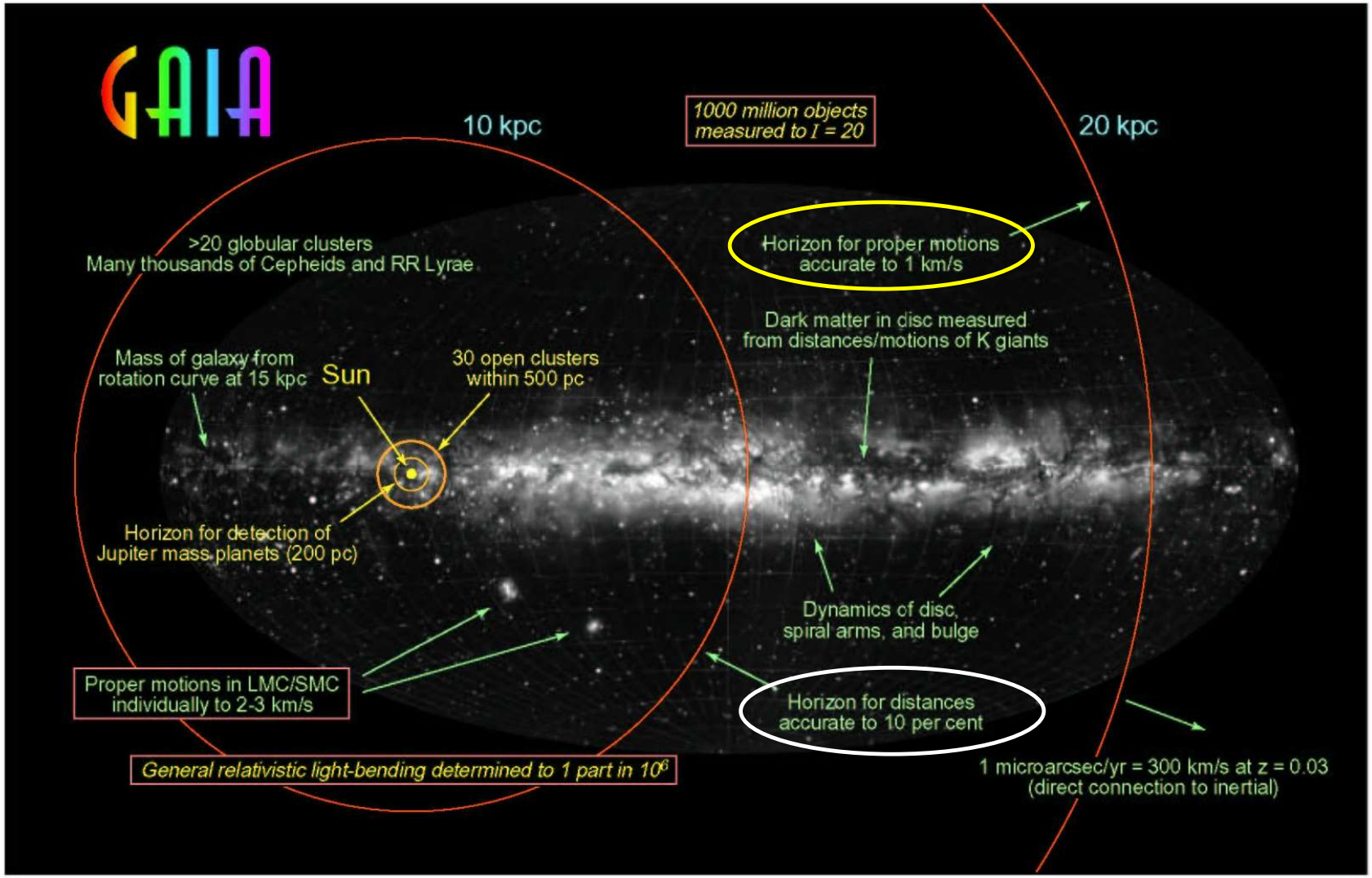

Gaia: 10μas = 10% error @distance 10kpc, 10μas/yr = 1km/s @20kpc

Hipparcos: 1mas = 10% error @distance 100pc, 1mas/yr = 5km/s @ 1kpc

Photometric Systems

M. Bessel 2005 ARAA, 43, 293

TABLE 1 Wavelengths (Å) and widths (Å) of broad-band systems

UBVRI			Washington			SDSS			Hipparcos			WFPC2		
	λeff	Δλ		λeff	Δλ		λeff	Δλ		λeff	Δλ		λeff	Δλ
U	3663	650	C	3982	1070	u'	3596	570	H_P	5170	2300	F336	3448	340
B	4361	890	M	5075	970	g'	4639	1280	B_T	4217	670	F439	4300	720
V	5448	840	T_1	6389	770	r'	6122	1150	V_T	5272	1000	F555	5323	1550
R	6407	1580	T_2	8051	1420	i'	7439	1230				F675	6667	1230
I	7980	1540				z'	8896	1070				F814	7872	1460

TABLE 3 Wavelengths (Å) and widths (Å) of intermediate-band systems

Strömgren			DDO			Geneva			Vilnius			Walraven		
	λeff	Δλ		λeff	Δλ		λeff	Δλ		λeff	Δλ		λeff	Δλ
u	3520	314	35	3460	383	U	3438	170	U	3450	400	W	3255	143
v	4100	170	38	3815	330	B	4248	283	P	3740	260	U	3633	239
b	4688	185	41	4166	83	$B1$	4022	171	X	4050	220	L	3838	227
y	5480	226	42	4257	73	$B2$	4480	164	Y	4660	260	B	4325	449
β_w	4890	150	45	4517	76	V	5508	298	Z	5160	210	V	5467	719
β_n	4860	30	48	4886	186	$V1$	5408	202	V	5440	260			
			51	5132	162	G	5814	206	S	6560	200			

M. Bessel 2005 ARAA, 43, 293

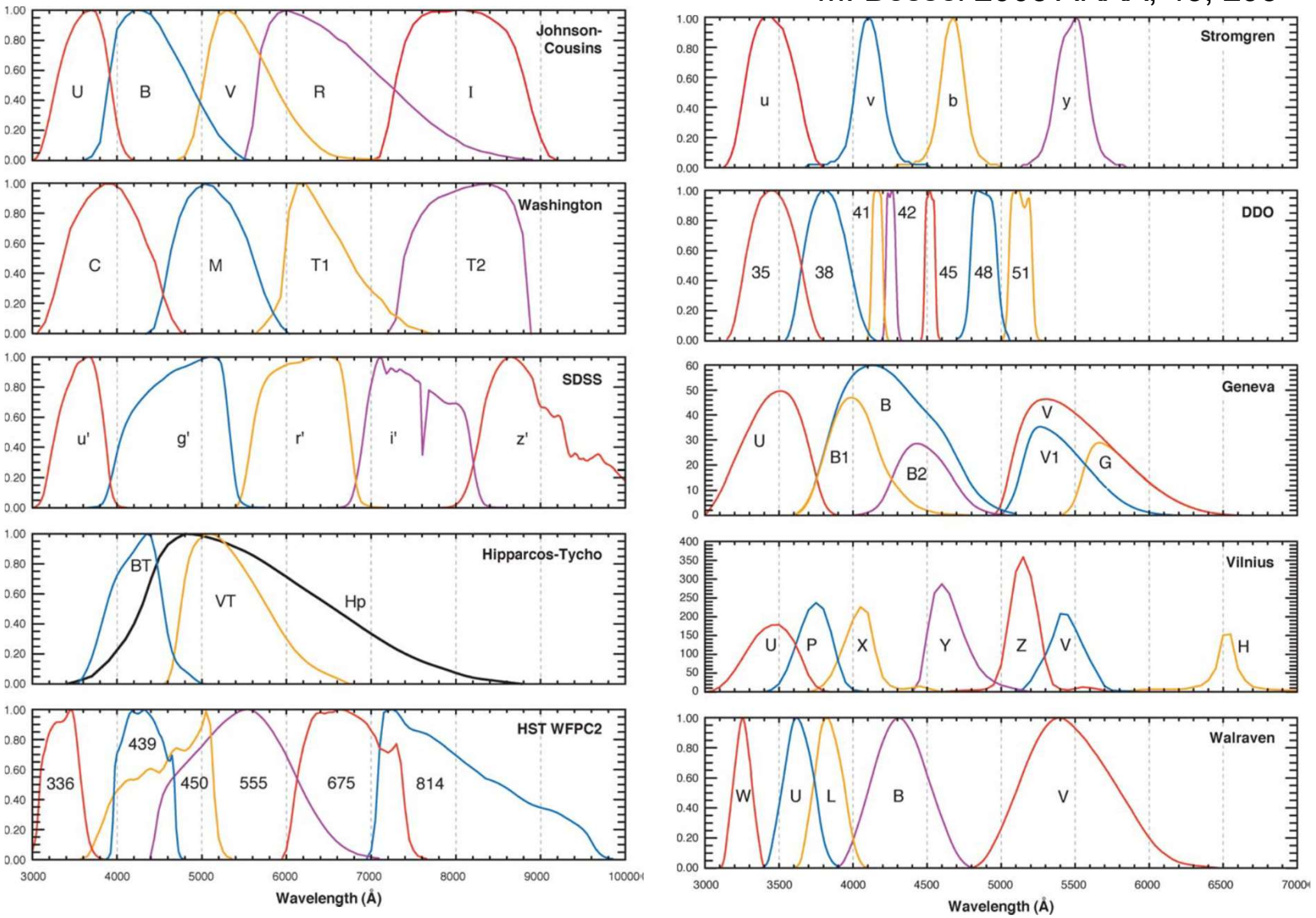

ヒッパルコス衛星による太陽近傍星の色－等級図

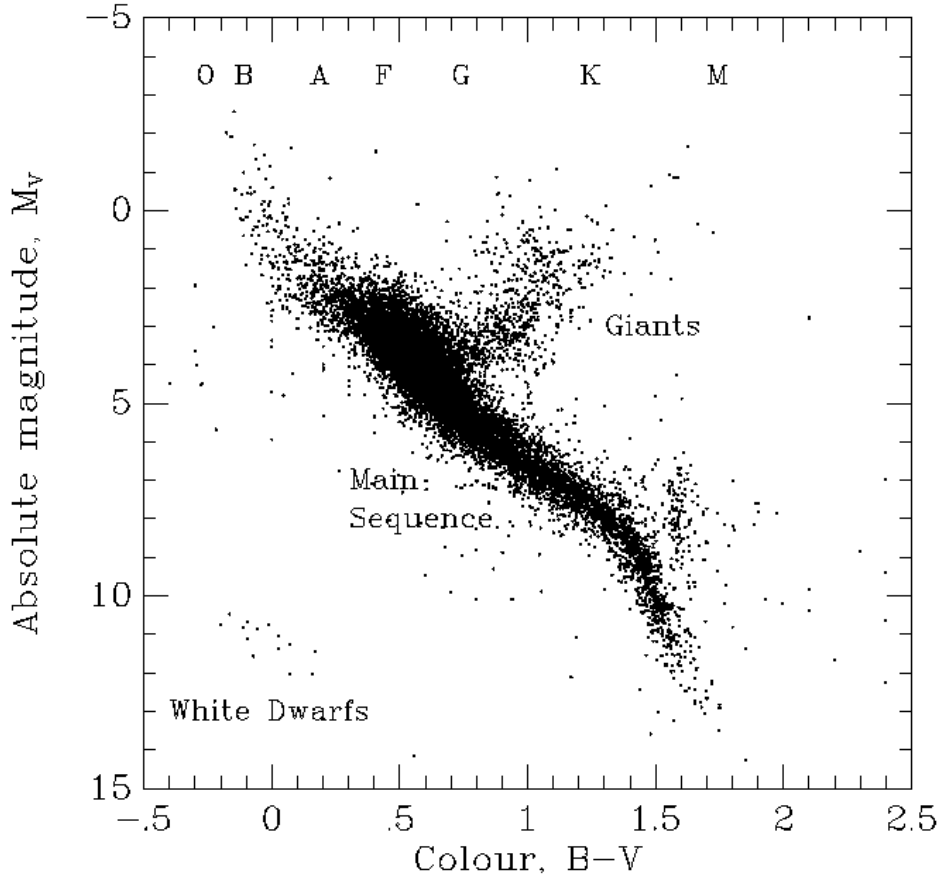

三角視差の相対エラー ＜ 10%

ガイア衛星による太陽近傍星の色－等級図

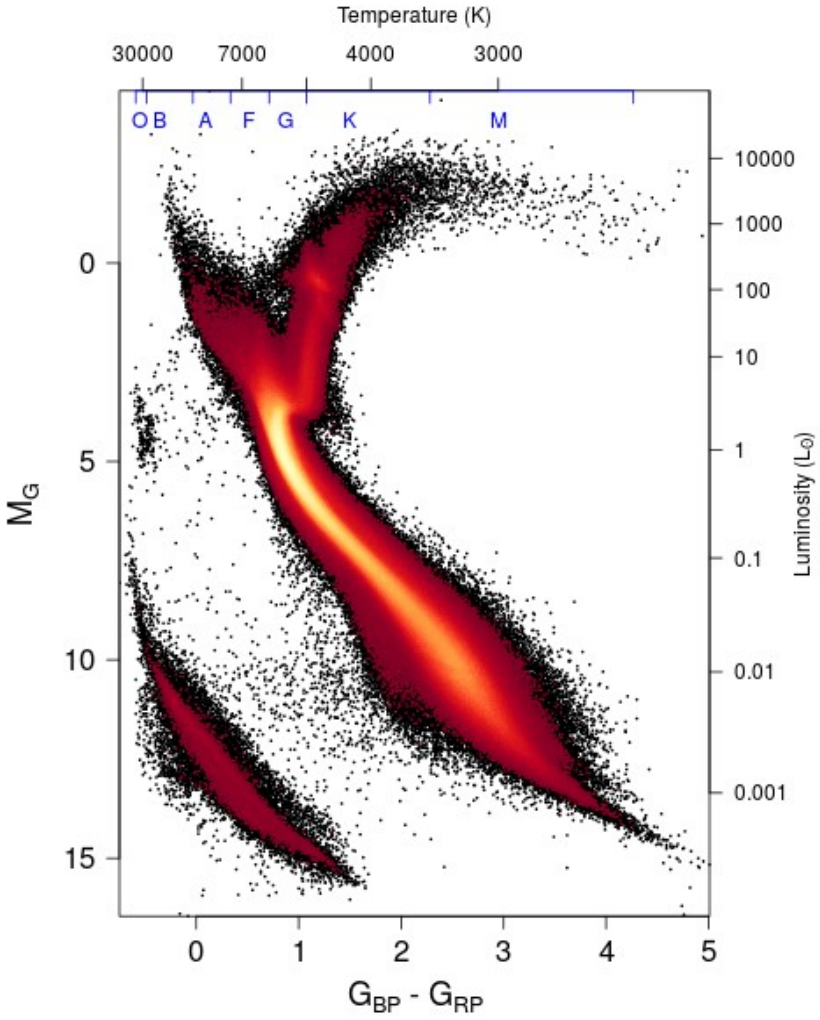

Gaia HRD of sources with low extinction (E(B − V) < 0.015 mag) satisfying the filters described in Sect. 2.1 (4,276,690 stars). The colour scale represents the square root of the density of stars. Approximate temperature and luminosity equivalents for main-sequence stars are provided at the top and right axis, respectively, to guide the eye.

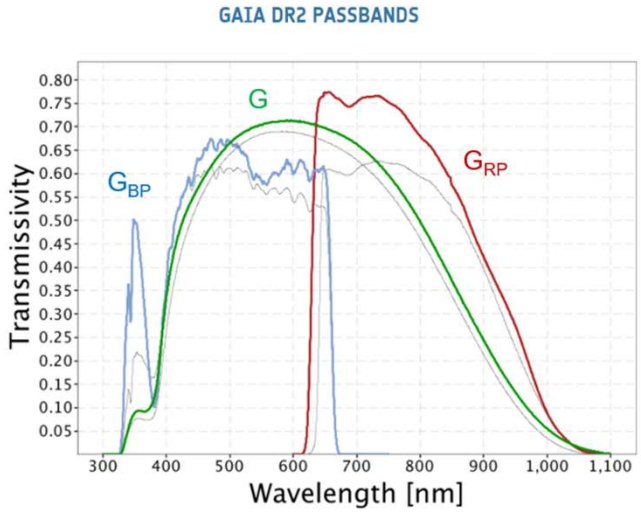

The coloured lines in the figure show the revised passbands for G, G_{BP} and G_{RP} (green: G; blue: G_{BP}; red: G_{RP}), defining the Gaia DR2 photometric system. The thin, grey lines show the nominal, pre-launch passbands published in Jordi et al. 2010, used for Gaia DR1.

ハローにある球状星団内の色－等級図

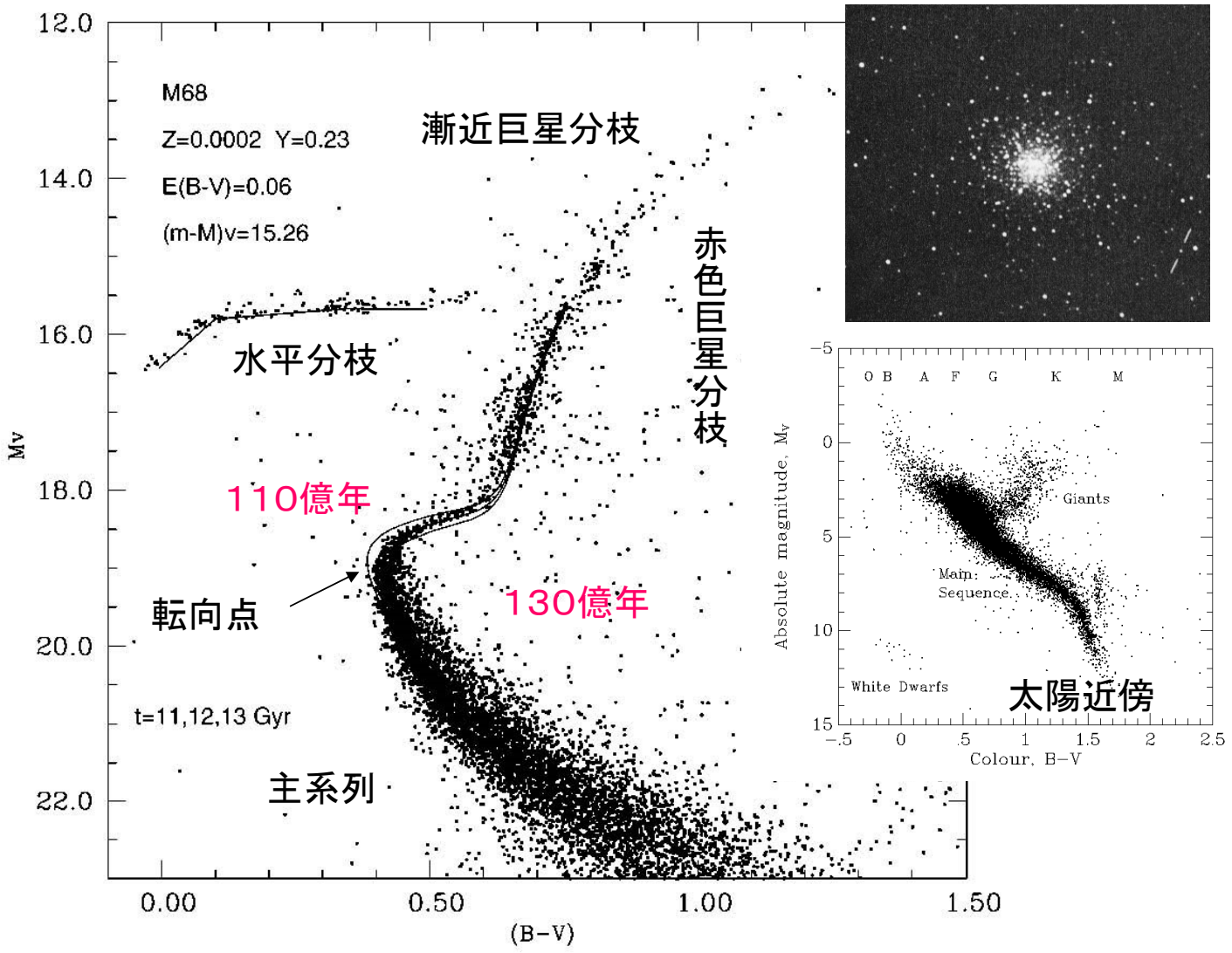

恒星の種族	年齢	空間運動	空間分布	金属量 （ヘリウムよりも重い元素量）
種族I (Population I) 渦状腕, 散開星団	若い	ほぼ円軌道	平坦	多い
種族II (Population II) バルジ, ハロー, 球状星団	古い	ランダム	球状	少ない（バルジを除く）
種族III (Population III)	古い	?	?	ゼロ

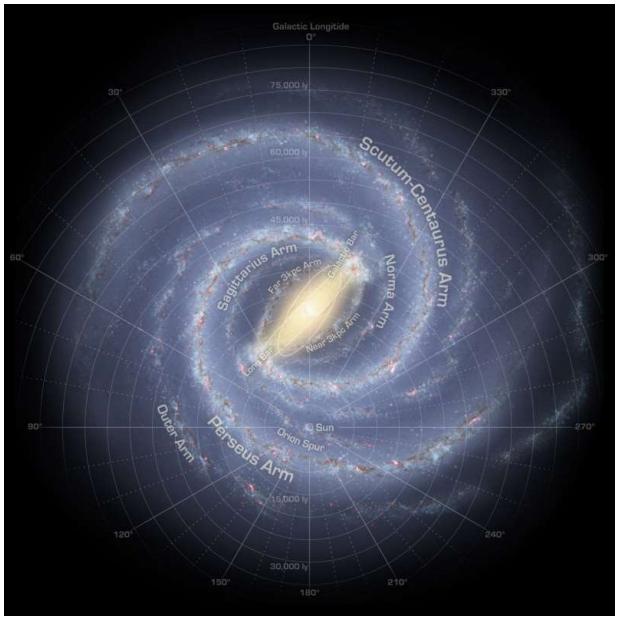

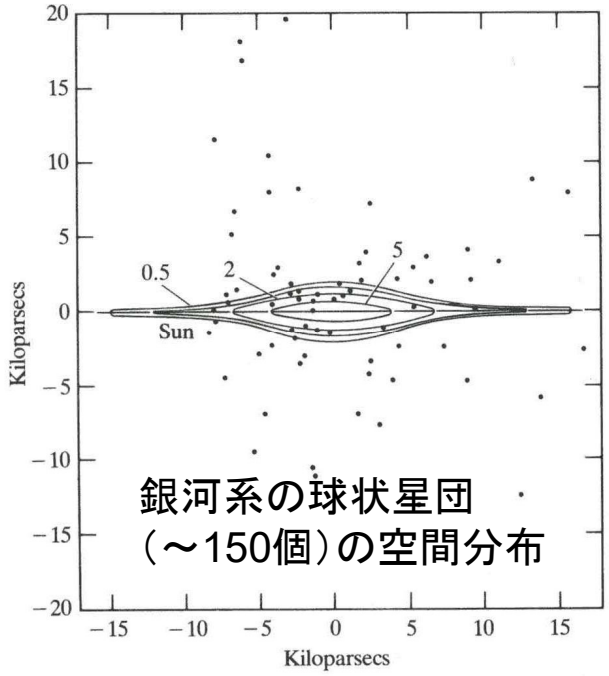

銀河系の球状星団
（～150個）の空間分布

SDSSによる銀河系F型星の低分散スペクトル

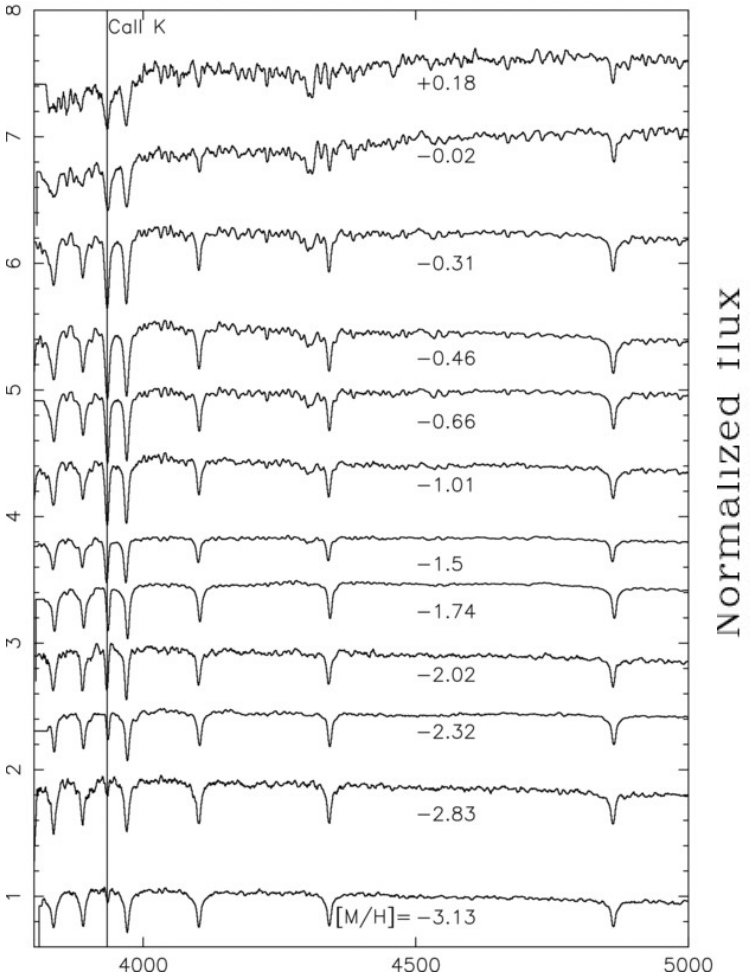

すばる望遠鏡による銀河系ハロー星の高分散スペクトル

High Dispersion Spectrograph (HDS)

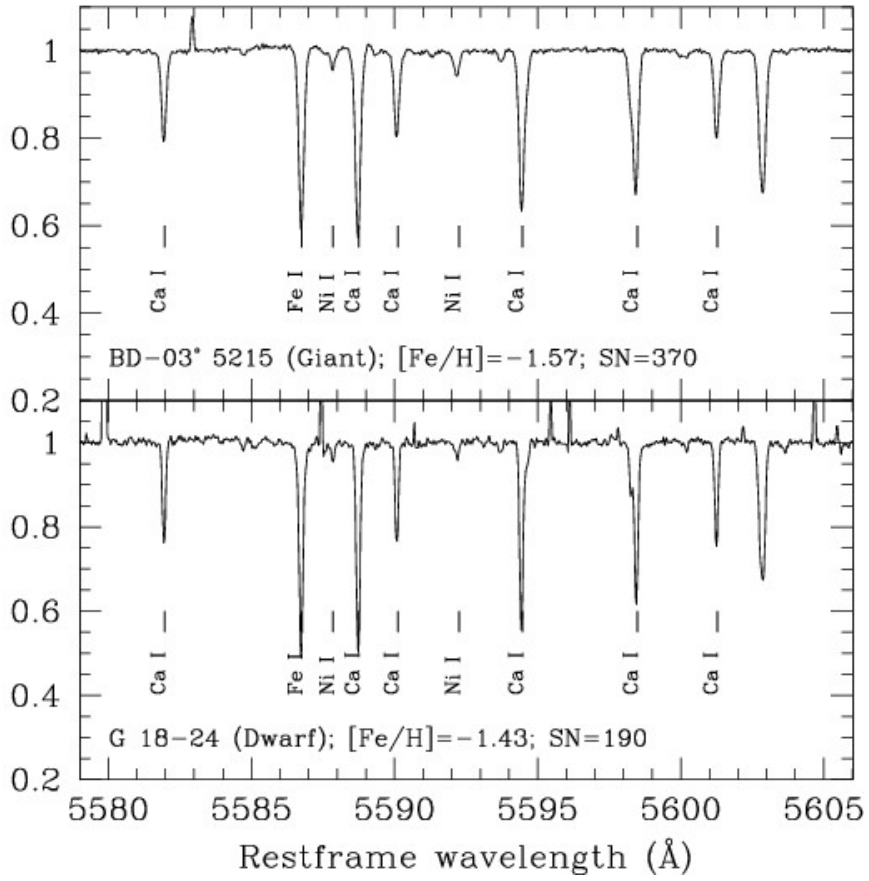

太陽のX, Y, Z (X+Y+Z=1)

Asplund et al. 2009, ARAA

Table 4: The mass fractions of hydrogen (X), helium (Y) and metals (Z) for a number of widely-used compilations of the solar chemical composition.

Source	X	Y	Z	Z/X
Present-day photosphere:				
Anders & Grevesse (1989)[a]	0.7314	0.2485	0.0201	0.0274
Grevesse & Noels (1993)[a]	0.7336	0.2485	0.0179	0.0244
Grevesse & Sauval (1998)	0.7345	0.2485	0.0169	0.0231
Lodders (2003)	0.7491	0.2377	0.0133	0.0177
Asplund, Grevesse & Sauval (2005)	0.7392	0.2485	0.0122	0.0165
Lodders, Palme & Gail (2009)	0.7390	0.2469	0.0141	0.0191
Present work	0.7381	0.2485	0.0134	0.0181
Proto-solar:				
Anders & Grevesse (1989)	0.7096	0.2691	0.0213	0.0301
Grevesse & Noels (1993)	0.7112	0.2697	0.0190	0.0268
Grevesse & Sauval (1998)	0.7120	0.2701	0.0180	0.0253
Lodders (2003)	0.7111	0.2741	0.0149	0.0210
Asplund, Grevesse & Sauval (2005)	0.7166	0.2704	0.0130	0.0181
Lodders, Palme & Gail (2009)	0.7112	0.2735	0.0153	0.0215
Present work	0.7154	0.2703	0.0142	0.0199

[a] The He abundances given in Anders & Grevesse (1989) and Grevesse & Noels (1993) have here been replaced with the current best estimate from helioseismology (Sect. 3.9).

非常に金属量が少ない星（超金属欠乏星）

[Fe/H] ≤ -2.5

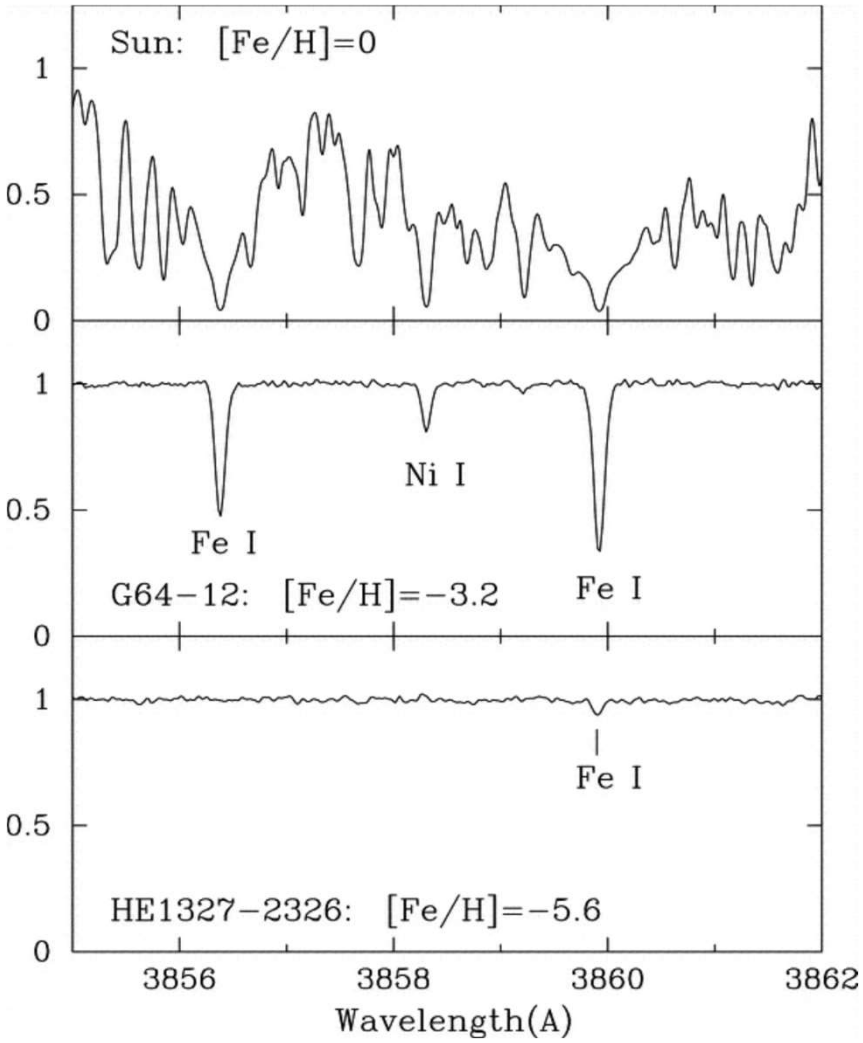

様々な球状星団の色－等級図

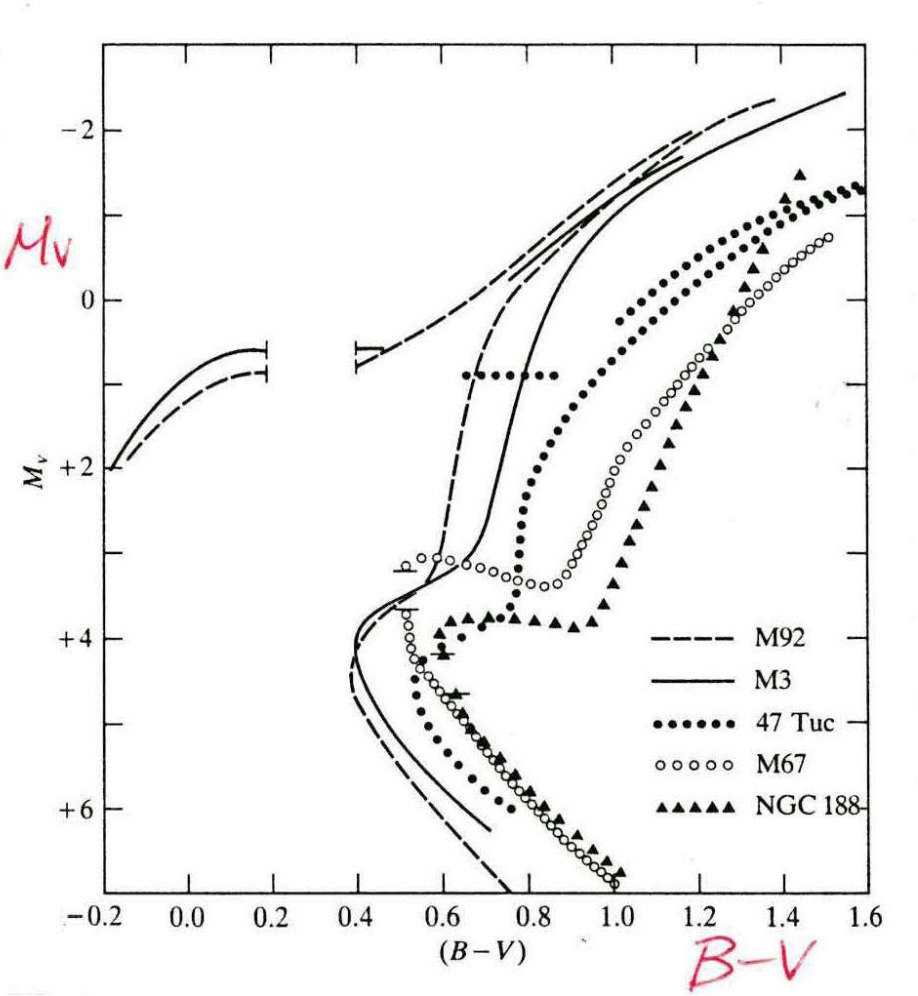

星団名	[Fe/H]
M92	-2.24
47 Tuc	-0.71
NGC188	-0.06

銀河の形態分類
ハッブルの音さ図（Tuning Fork）

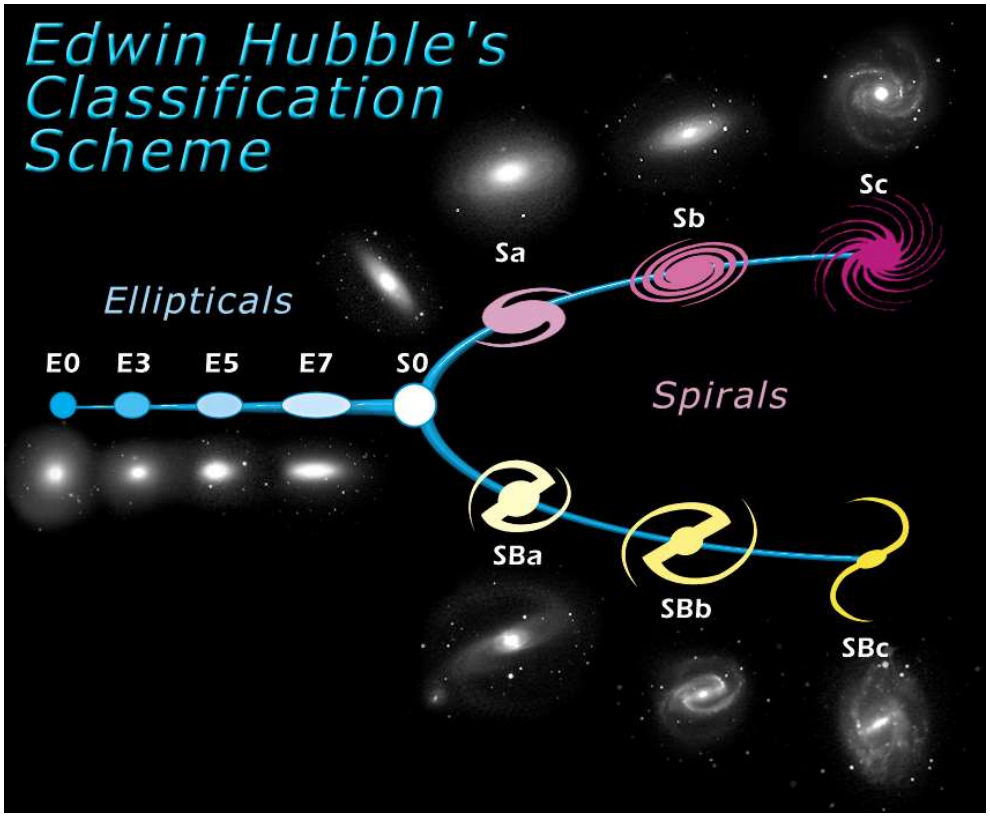

早期型
early-type

晩期型
late-type

星間ガスの量多い
L_bulge/L_disk が小さい
腕(arm)の巻き込みがゆるい
色が青い（B-V↓）

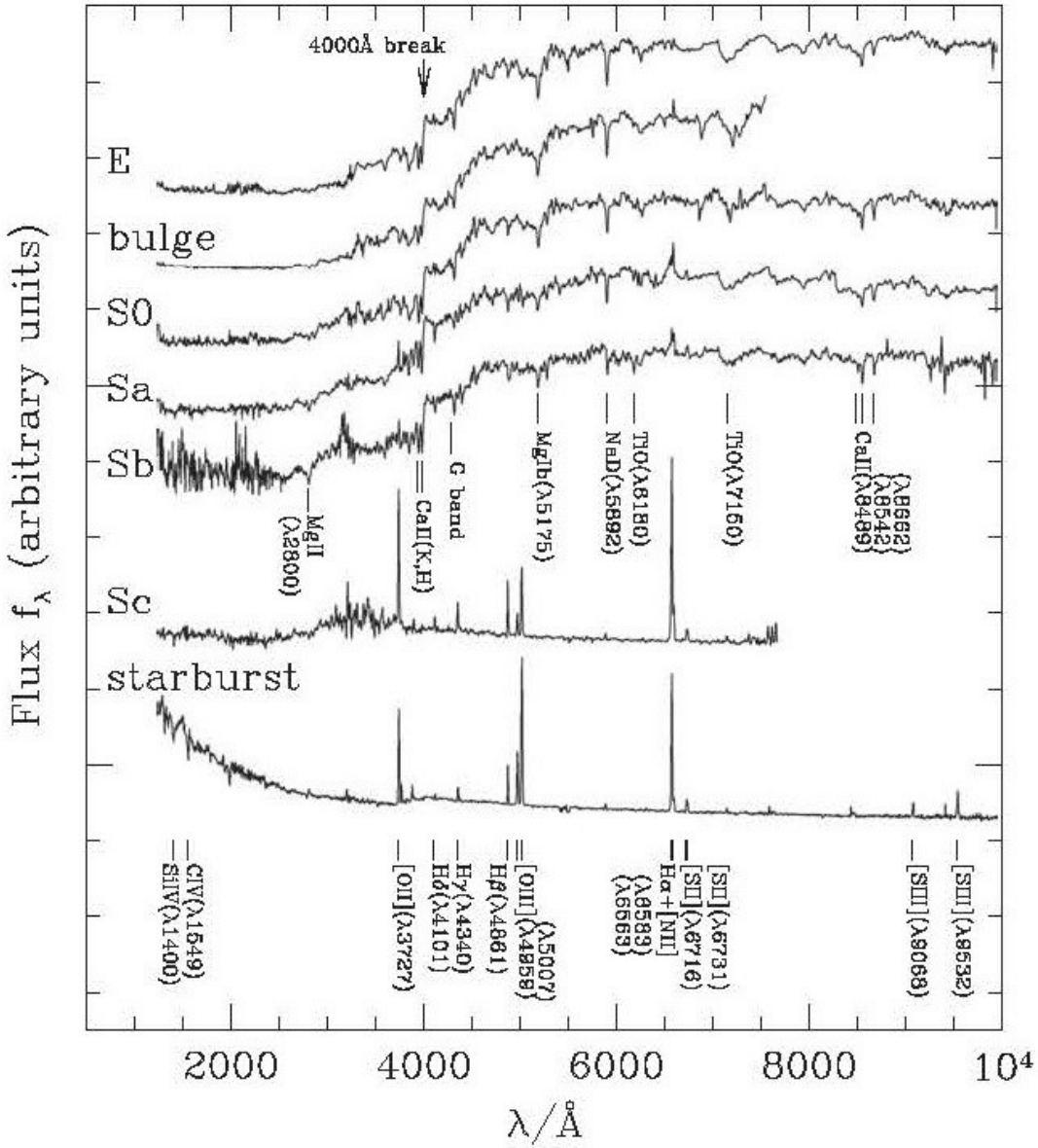
4000Å break
E
bulge
S0
Sa
Sb
Sc
starburst
Flux f_λ (arbitrary units)
MgII (λ2800)
CaII(K,H)
G band
MgIb(λ5175)
NaD(λ5892)
TiO(λ8180)
TiO(λ7150)
CaII(λ8489) {λ8662} {λ8542}
CIV(λ1549)
SiIV(λ1400)
[OII](λ3727)
Hδ(λ4101)
Hγ(λ4340)
Hβ(λ4861)
[OIII](λ4959) {λ5007}
[OI](λ6300) {λ6363}
Hα+[NII]
[SII](λ6716)
[SII](λ6731)
[SIII](λ9068)
[SIII](λ9532)
2000
4000
6000
8000
10^4
λ/Å

円盤銀河の表面輝度分布

$$I(R) = I_0 \exp(-R/R_d)$$ Exponential disk

$$\Rightarrow \mu \propto -\frac{5}{2}\log_{10} I \propto R/R_d$$

Boroson 1981
ApJS, 46, 177

表面輝度μ（等級/面積）

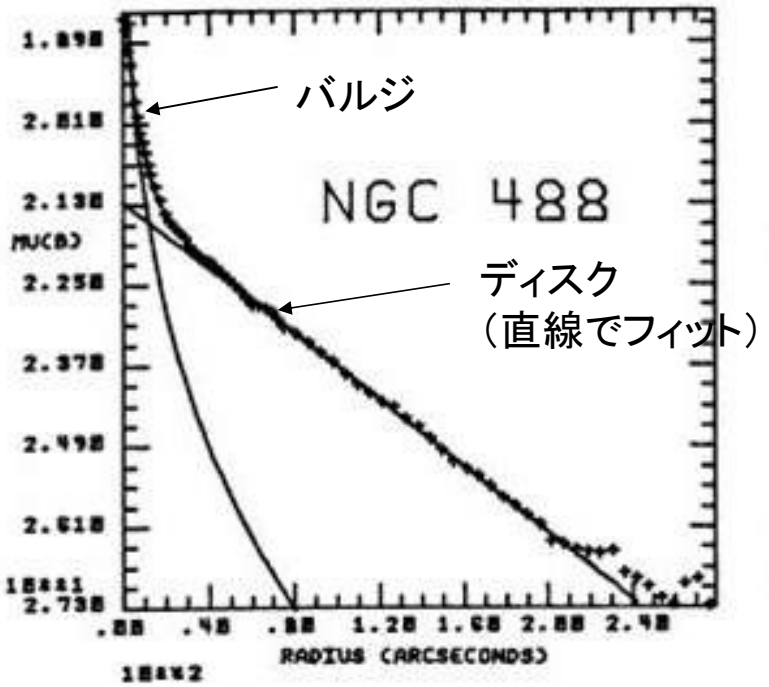

中心からの距離（角度秒）

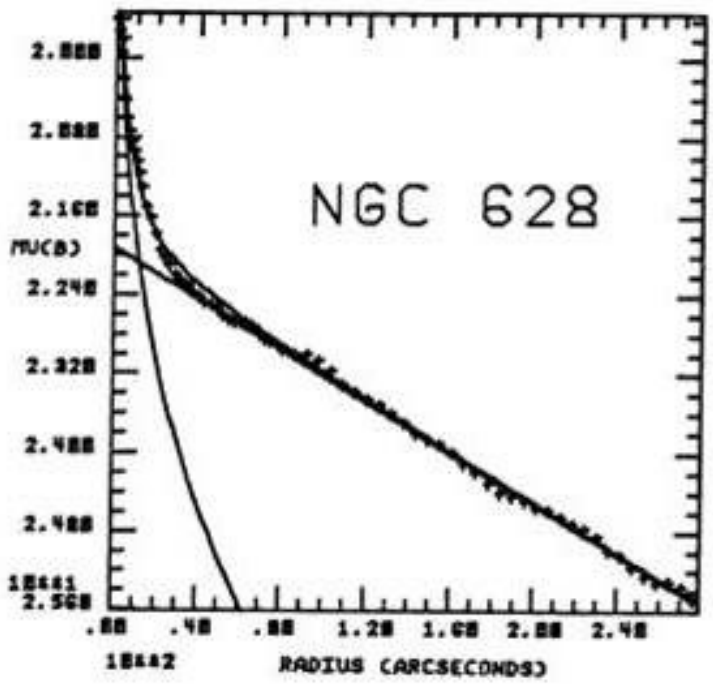

中心からの距離（角度秒）

銀河面に垂直方向の星の密度分布

Gilmore & Reid 1983, MN, 202, 1025

Discovery of the thick-disk component

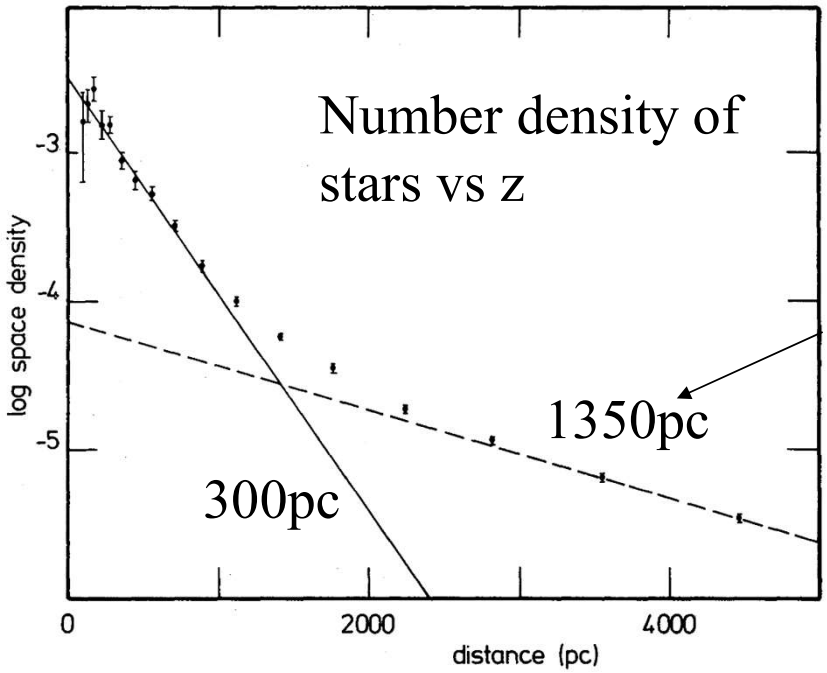

Exponential scale height h_z

	h_z(kpc)	σ_R(km/s)	σ_z(km/s)	<Vφ>(km/s)
Thin disk	~0.3	34	18	220
Thick disk	~1.0	61	39	200

NGC4565

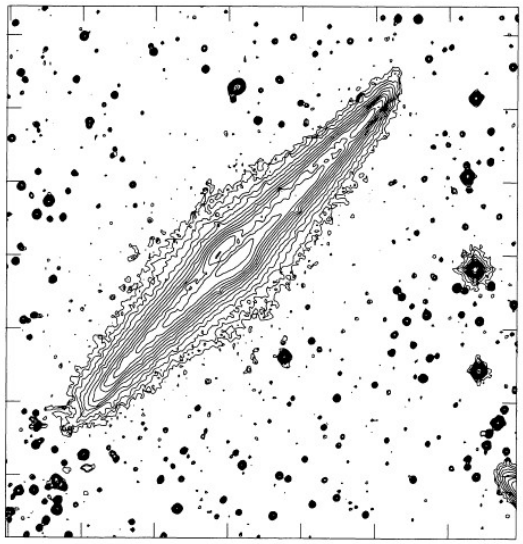

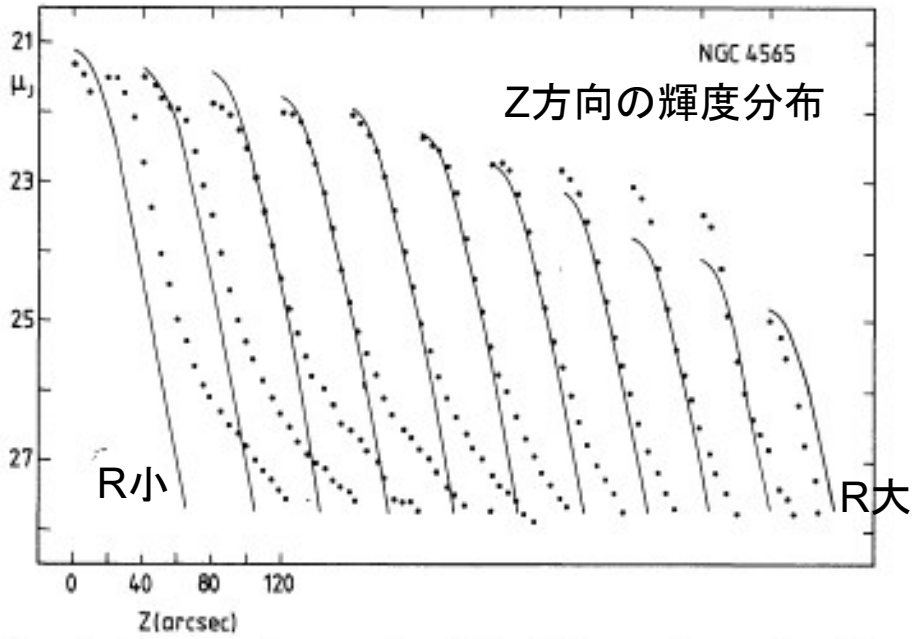

Fig. 12. The complete set of model and observed *z*-profiles after rectangle smoothing for NGC 4565. Note that from the third profiles outward the observed profiles have a linear part that is fitted in brightness and slope by the model. The shallowing of the observed profiles at fainter levels is similar to those of Burstein's "thick disks"

van der Kruit and Searle 1981

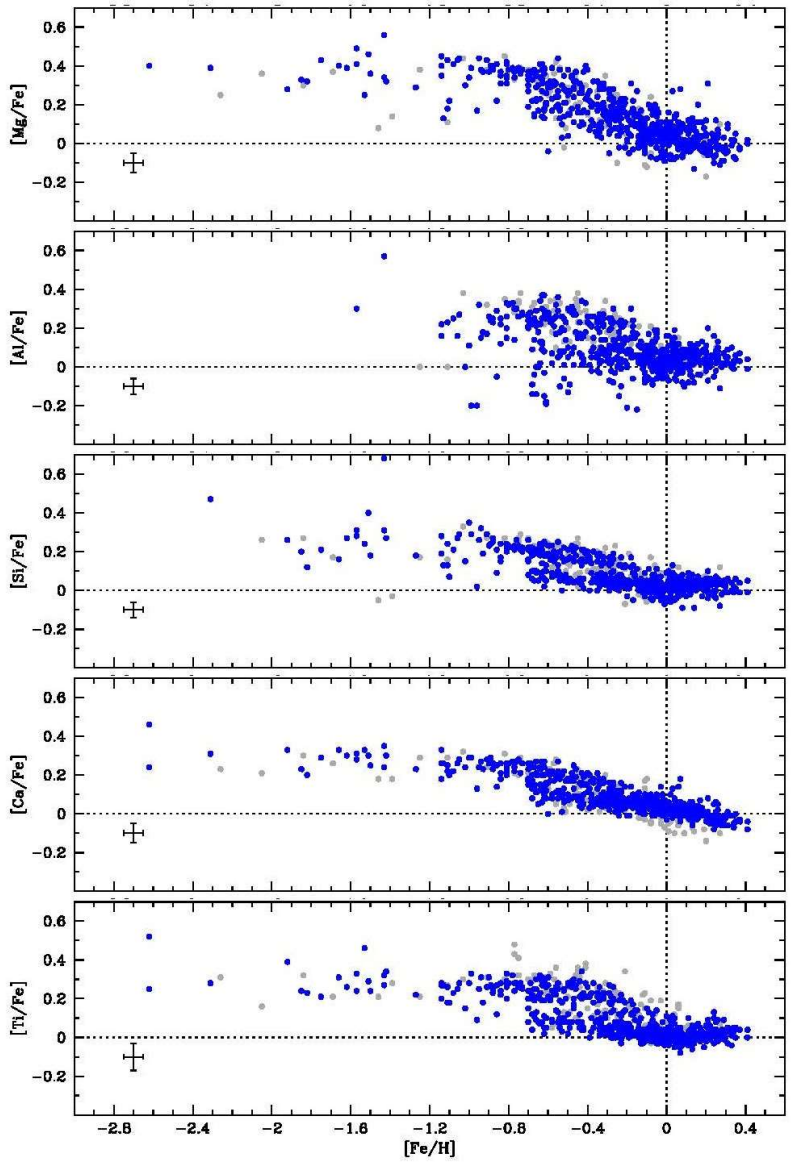

[alpha-elements/Fe]
= Type II SNe / Type Ia SNe

Chemical clock diagram

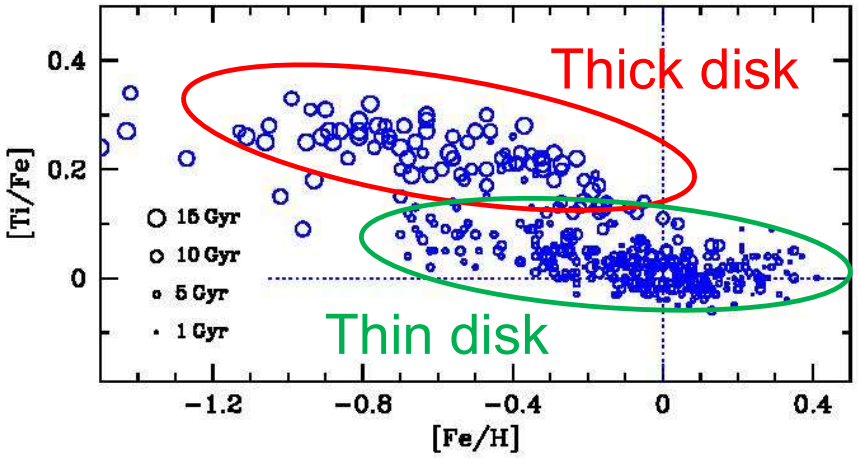

Bensby+ 2014

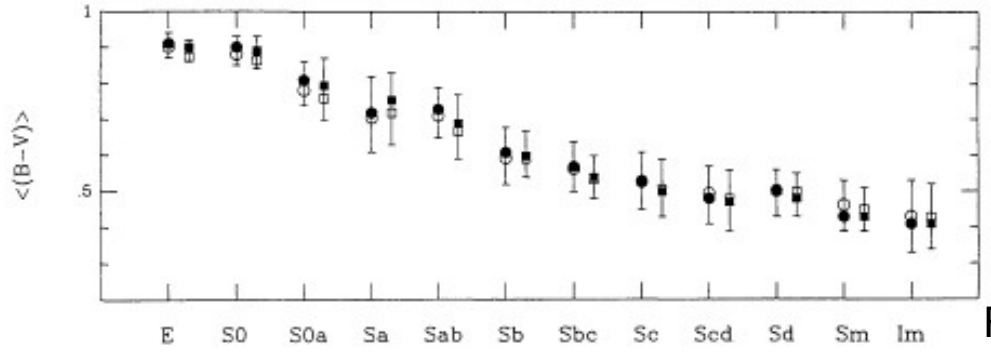

Figure 5 (B – V) color vs morphological type. (Same symbols as in Figure 2.)

RC3, UGC catalogs

Roberts & Haynes, 1994, ARAA, 32, 115

単位質量あたりの角運動量 (J/M)
vs. 光っている部分の質量 (M)

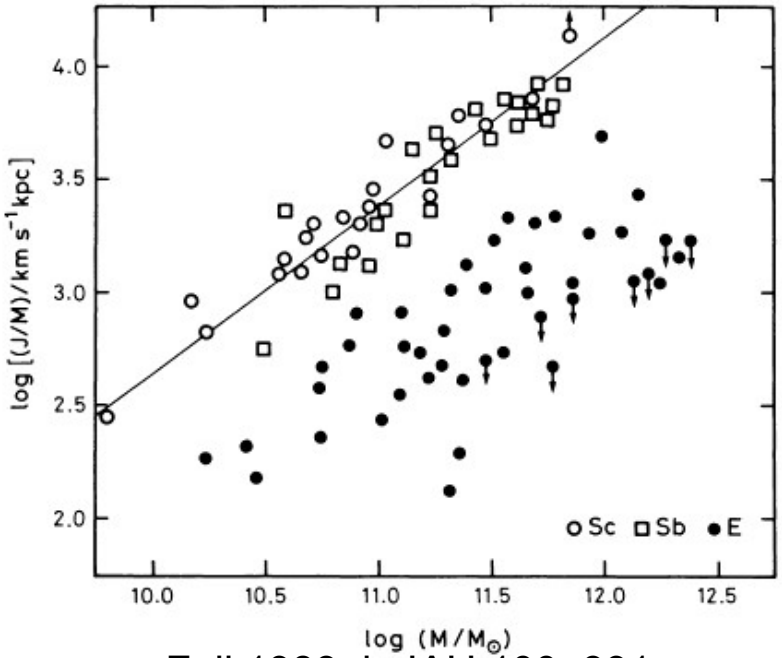

Fall 1983, in IAU 100, 391

Bulge L /Total L

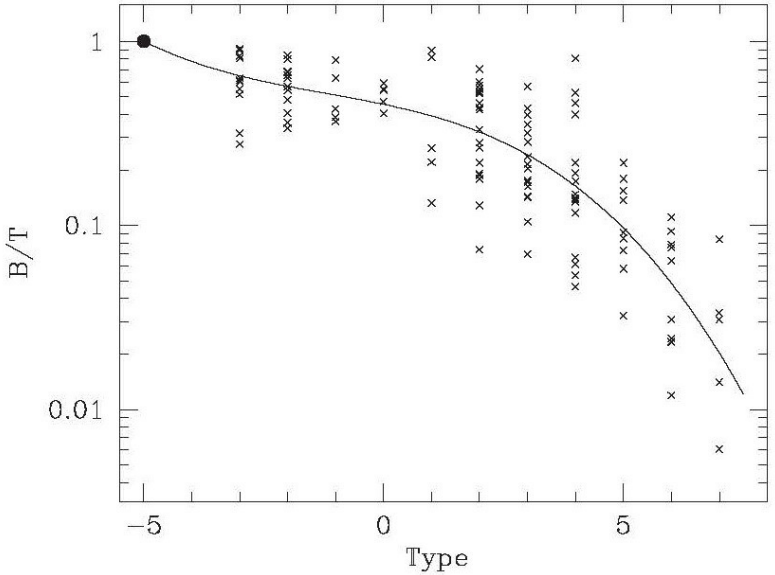

Simien & de Vaucouleurs 1986

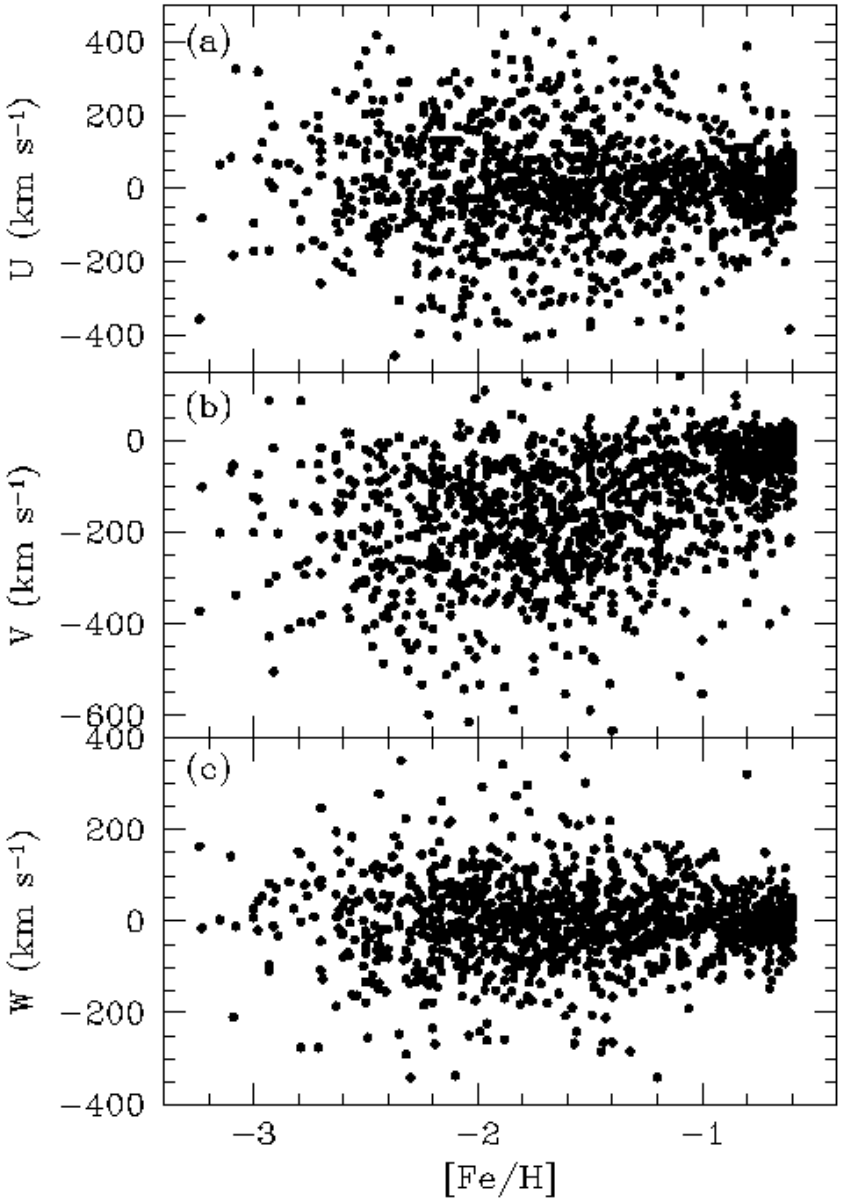

太陽近傍にある
金属欠乏星の
3次元速度分布

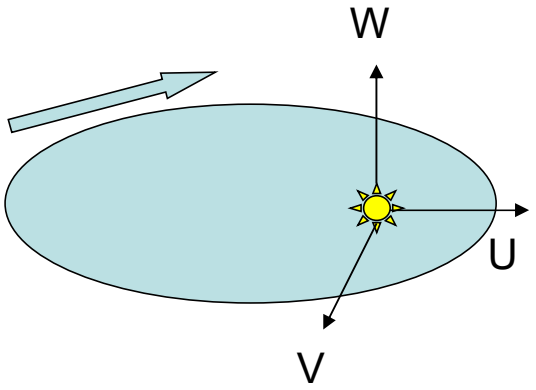

(U, V, W) 速度成分:
約220km/sで円運動する系
局所静止基準
Local Standard of Rest (LSR)
からみた速度

球状星団の空間分布

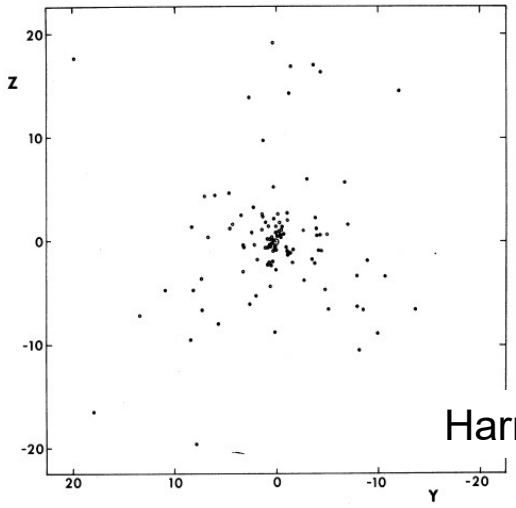

Harris 1976

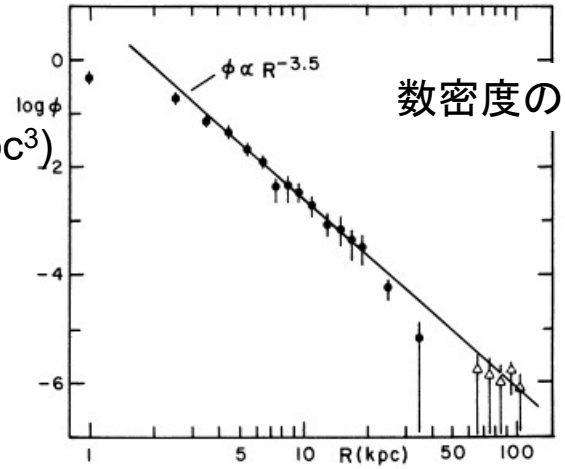

数密度の r 依存

FIG. 2.—The number of clusters per cubic kiloparsec (ϕ) is plotted against galactocentric distance (R). The solid circles represent the clusters with $|Z| < 20$ kpc; the open triangles represent the clusters with $|Z| > 37$ kpc. There are no clusters in the zone $33 < R < 60$ kpc.

Zinn 1985

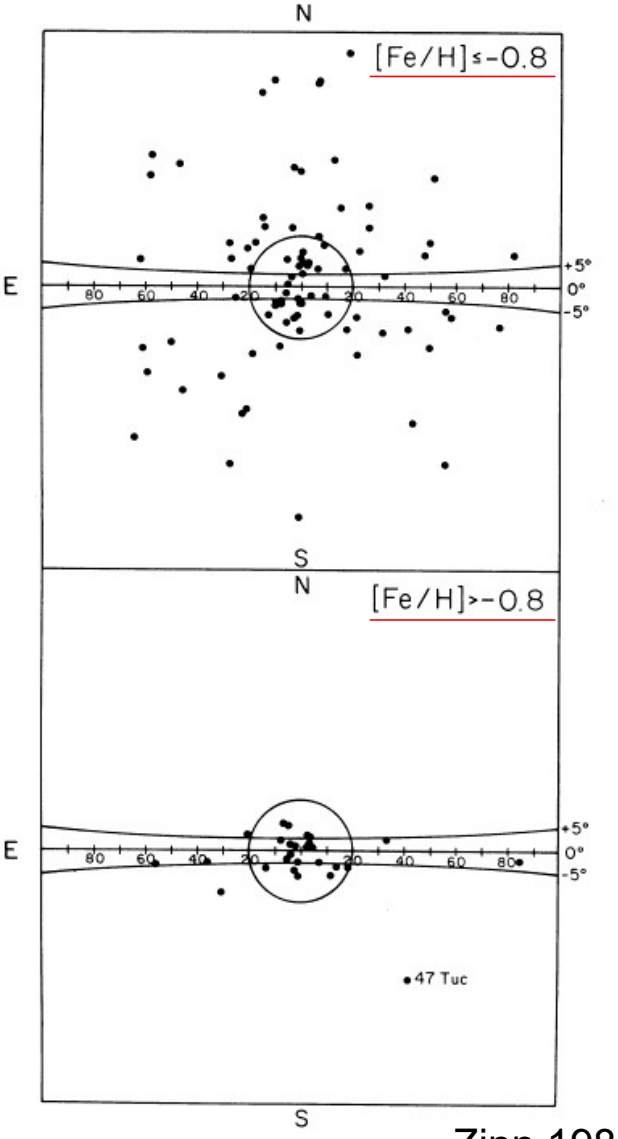

Zinn 1985

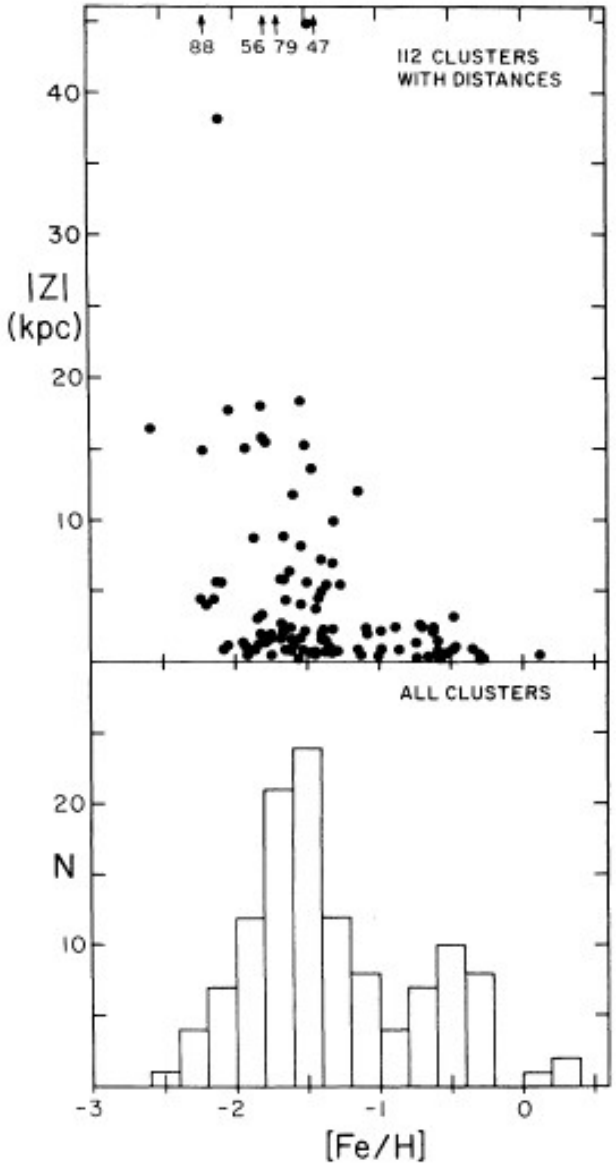
88
56 79 47
112 CLUSTERS
WITH DISTANCES
40
30
|Z|
(kpc)
20
10
ALL CLUSTERS
20
N
10
-3
-2
-1
0
[Fe/H]

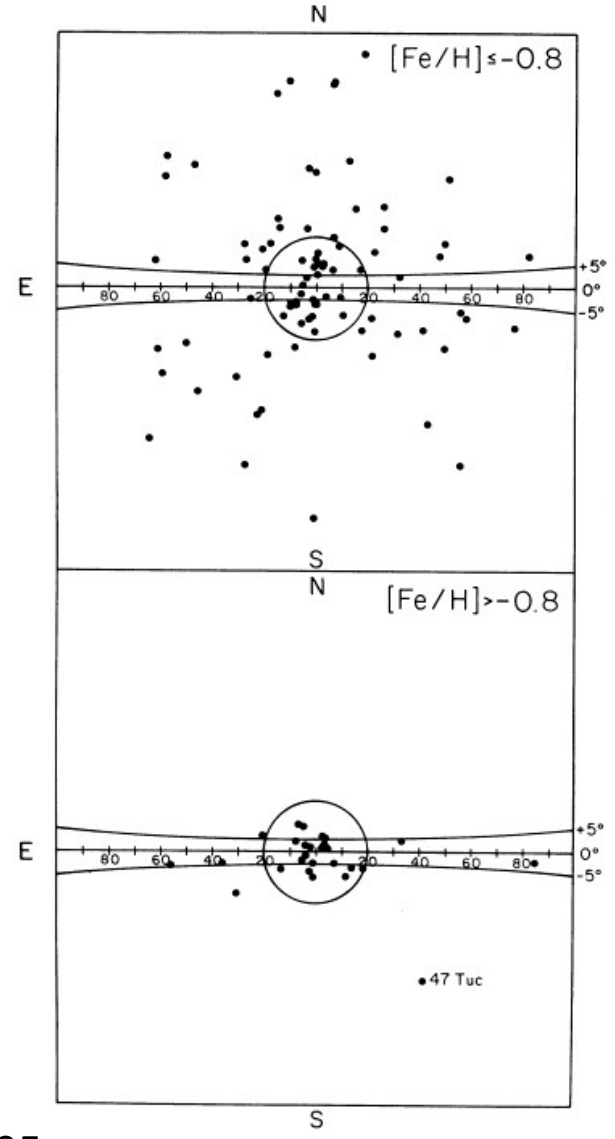
N
[Fe/H]≤-0.8
E
+5°
0°
-5°
S
N
[Fe/H]>-0.8
E
+5°
0°
-5°
47 Tuc
S

Zinn 1985

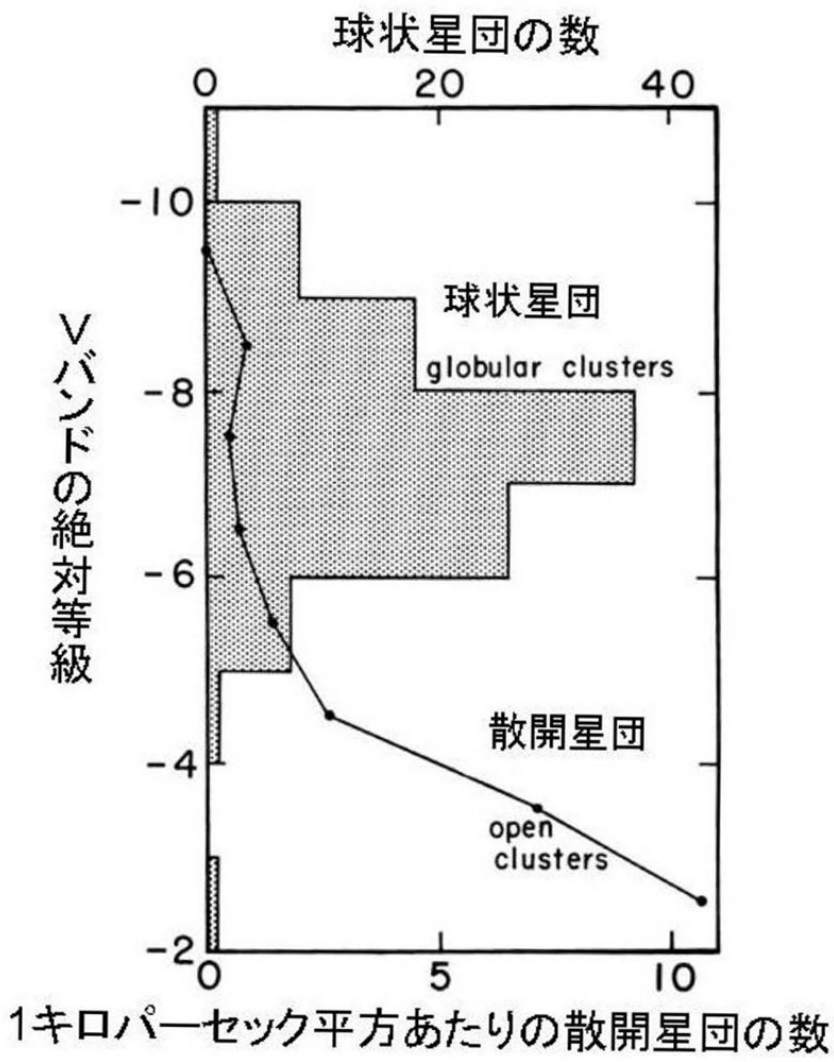

球状星団 Omega Centauri

散開星団　NGC290

Bulge

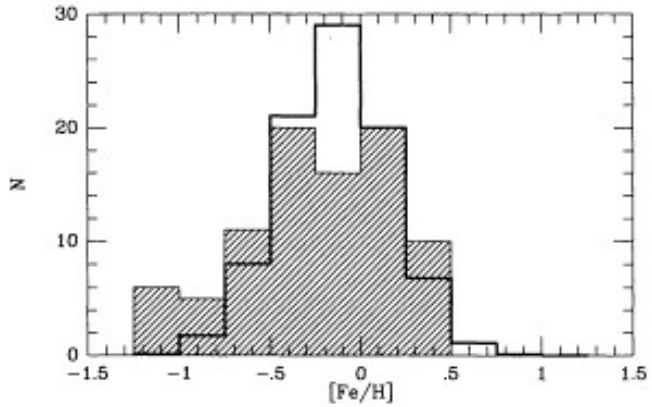

McAilliam & Rich 1994

FIG. 17.—The hatched area represents a frequency histogram of Rich (1988) solution 1 [Fe/H], corrected for the regression relation found here. The solid histogram outline represents the solar neighborhood GK giant distribution found by McWilliam (1990), smoothed by a Gaussian of σ = 0.25 dex. Note that the bulge giants have a similar mean [Fe/H] but a slightly broader distribution and more very metal-poor stars.

Halo stars

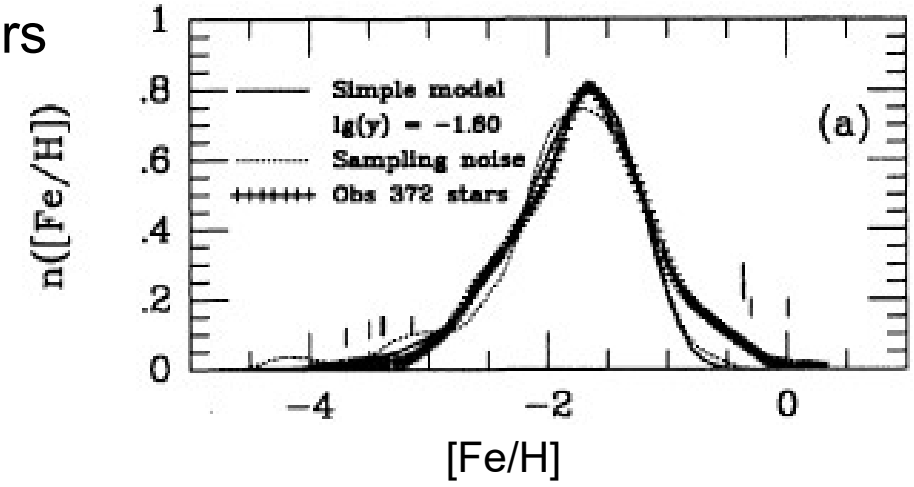

Ryan & Norris 1991

表面輝度

回転曲線

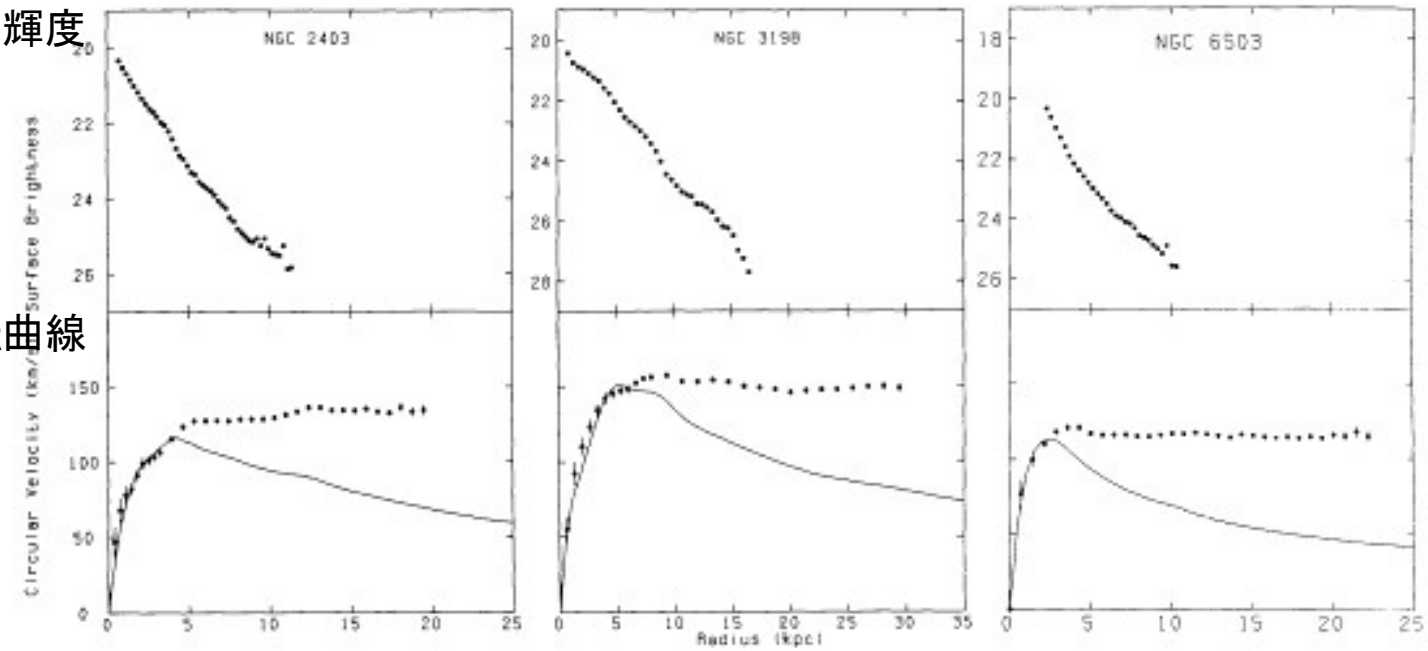

Radius (kpc)

Figure 2. Light profiles and rotation curves for three spiral galaxies with extended, symmetrical HI disks. Upper panels: luminosity profiles from Wevers (1984). Lower panels: HI rotation curves (dots with error bars, Begeman 1986) and curves representing the circular velocity of stars and gas (solid line). The light contribution has been calculated from the luminosity profile by assuming that M/L is constant with radius and has the maximum value allowed by the observed rotation curve.

Sancisi & van Albada 1987, IAU 117

Determination of the rotation curve

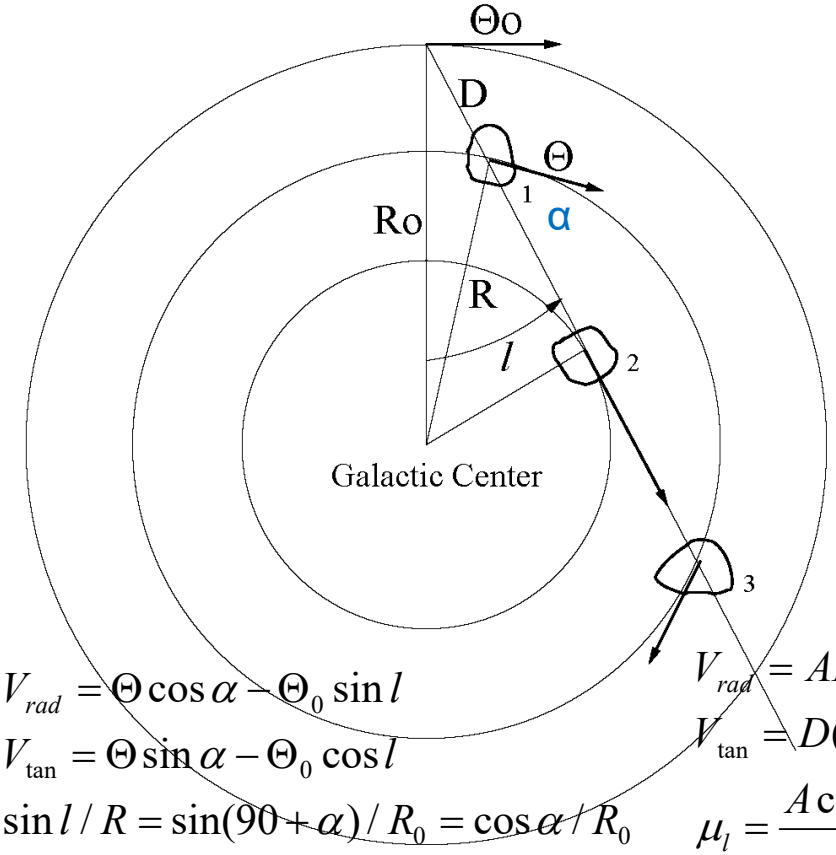

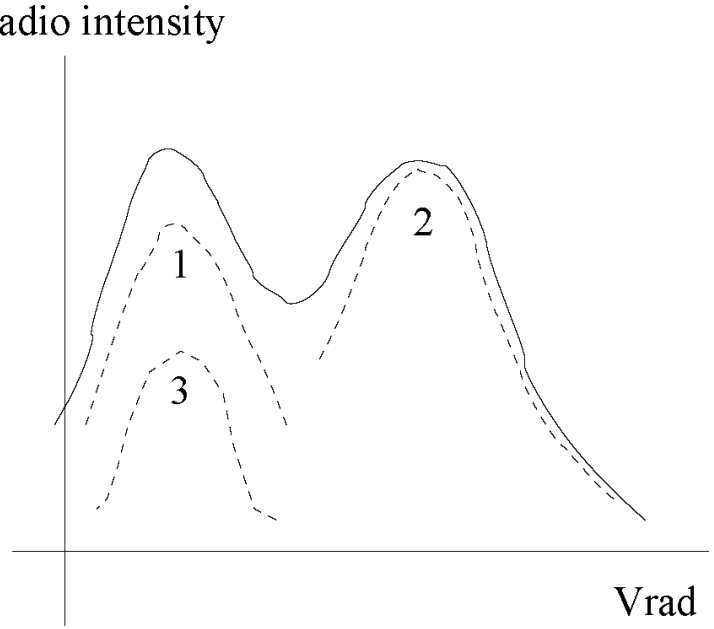

$$V_{rad} = \Theta \cos\alpha - \Theta_0 \sin l$$

$$V_{\tan} = \Theta \sin\alpha - \Theta_0 \cos l$$

$$\sin l / R = \sin(90+\alpha)/R_0 = \cos\alpha / R_0$$

$$R\cos(90-\alpha) = R\sin\alpha = R_0 \cos l - D$$

$$V_{rad} = (\Omega - \Omega_0) R_0 \sin l$$

$$V_{\tan} = (\Omega - \Omega_0) R_0 \cos l - \Omega D$$

$\Rightarrow$ *(R_0-R)/R_0<<1* $\Rightarrow$

$$V_{rad} = AD \sin 2l$$

$$V_{\tan} = D(A\cos 2l + B)$$

$$\mu_l = \frac{A\cos 2l + B}{4.74}$$

$$A \equiv \frac{1}{2}\left[\frac{\Theta_0}{R_0} - \left(\frac{d\Theta}{dR}\right)_{R_0}\right]$$

$$B \equiv -\frac{1}{2}\left[\frac{\Theta_0}{R_0} + \left(\frac{d\Theta}{dR}\right)_{R_0}\right]$$

A, B: Oort Constants

$$\Omega_0 = \Theta_0 / R_0 = A - B$$

$$\left(\frac{d\Theta}{dR}\right)_{R_0} = -(A+B)$$

V_{rad} is max at $R = R_0 \sin l \Rightarrow \Theta(R)$

$$\frac{\partial V_{rad}}{\partial D} = 0 \Rightarrow \partial R/\partial D = 0$$

$$R^2 = D^2 + R_0^2 - 2DR_0\cos l$$

$$\Rightarrow D = R_0 \cos l \quad \Rightarrow R = R_0 \sin l$$

Rotation curve of the Milky Way

Sofue et al. 2009, PASJ, 61, 227

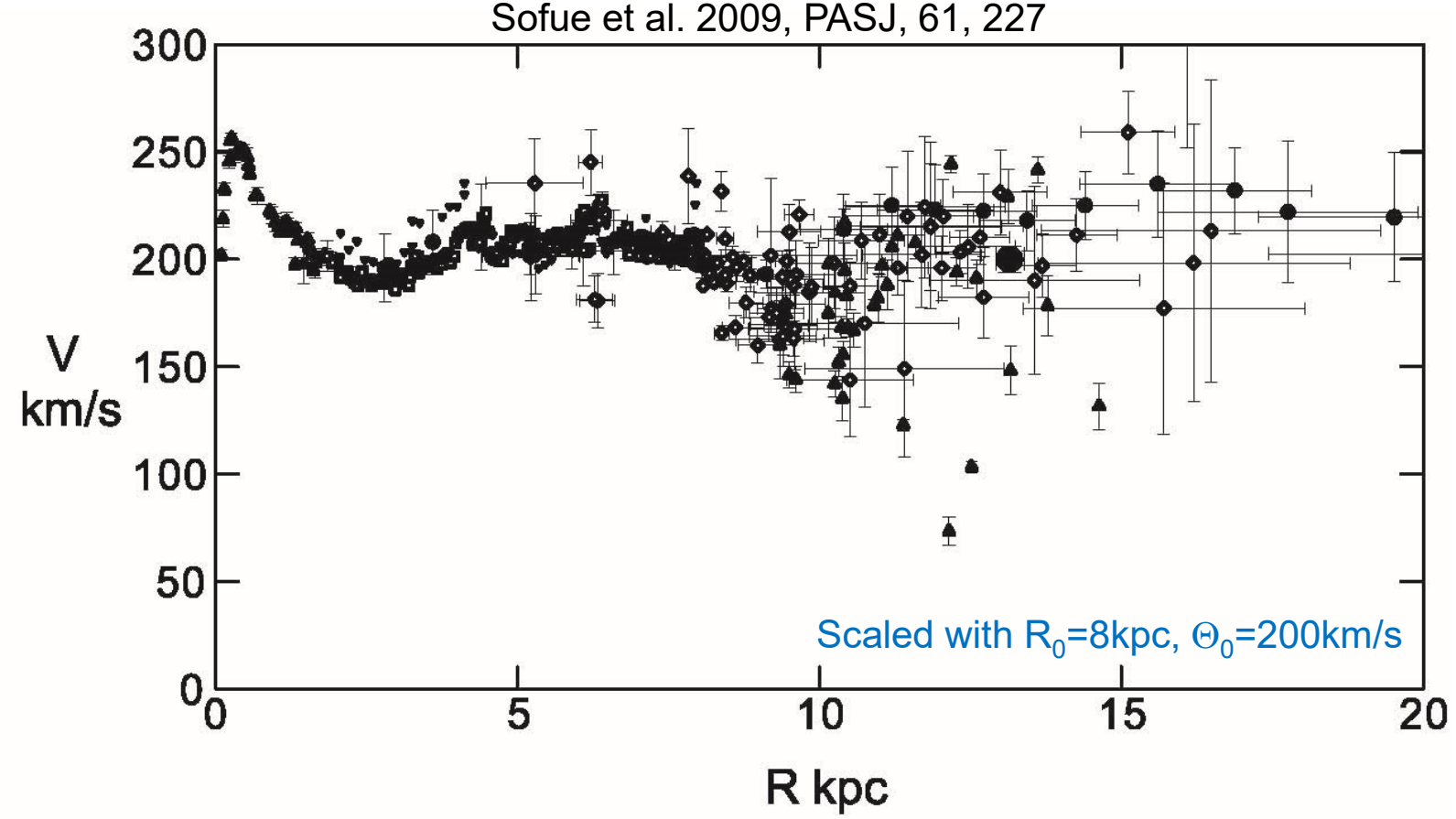

See also, Gunn, Knapp, Tremaine 1979, AJ, 84, 1181;
Fich & Tremaine 1991, ARAA, 29, 409

Honma et al. 2012, PASJ, 64, 136 VLBI Astrometry

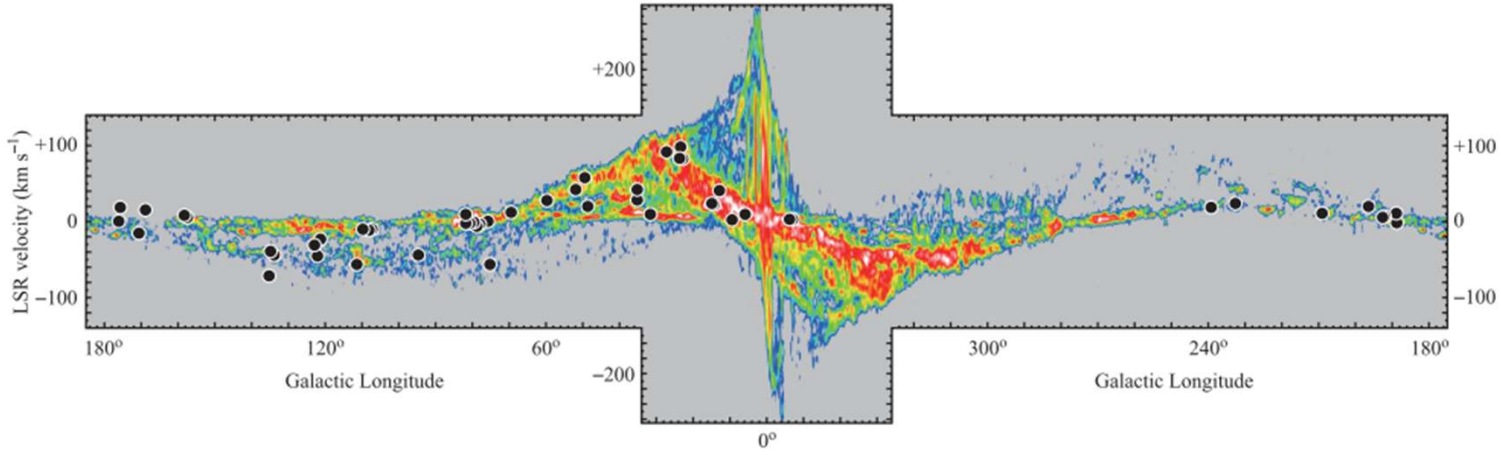

Fig. 1. Location of 52 maser sources for which accurate astrometric data are available (table 1), superposed on the longitude–velocity diagram of CO (Dame et al. 2001).

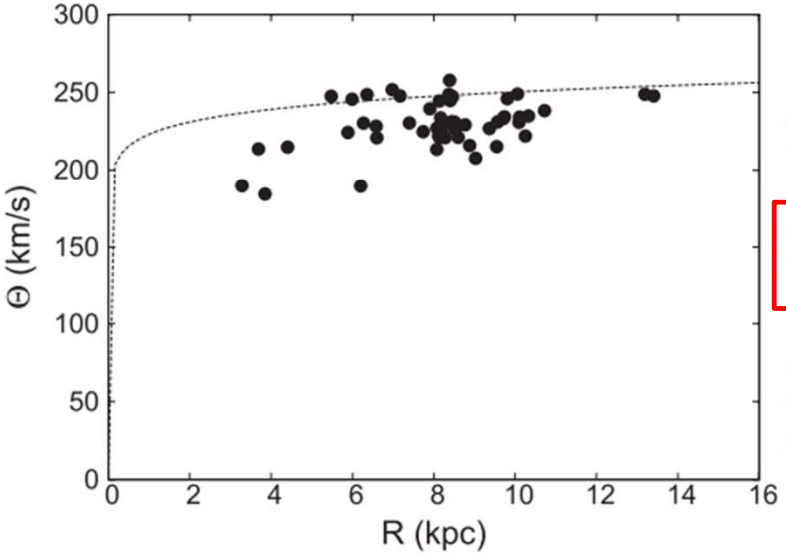

Fig. 6. Rotation curve plot for result 1 (52 sources). Filled circles correspond to the observed sources. Values of R_0 and Θ_0 are taken from the relevant results in table 1 ($R_0 = 8.27\,\mathrm{kpc}$, $\Omega_0 = 29.98\,\mathrm{km\,s^{-1}\,kpc^{-1}}$ and thus $\Theta_0 = R_0 \times \Omega_0 = 248\,\mathrm{km\,s^{-1}}$). Here error bars are not shown because in most cases they are invisibly small in this plot (but note that the systematic effect is considerably large as described in the text). Dotted line shows a rotation curve with $\Theta_0 = 248\,\mathrm{km\,s^{-1}}$ and a power-law index $\alpha = 0.05$. Note that here $V_\odot = 5.25\,\mathrm{km\,s^{-1}}$ is adopted and hence the lag of SFRs against Galactic rotation is prominent (by $\sim 15\,\mathrm{km\,s^{-1}}$), with most of data points located below the model rotation curve.

楕円銀河・バルジの輝度分布

$$I(R) = I_0 \exp(-kR^{1/4})$$

$$\mu \propto -\frac{5}{2}\log_{10} I \propto R^{1/4}$$

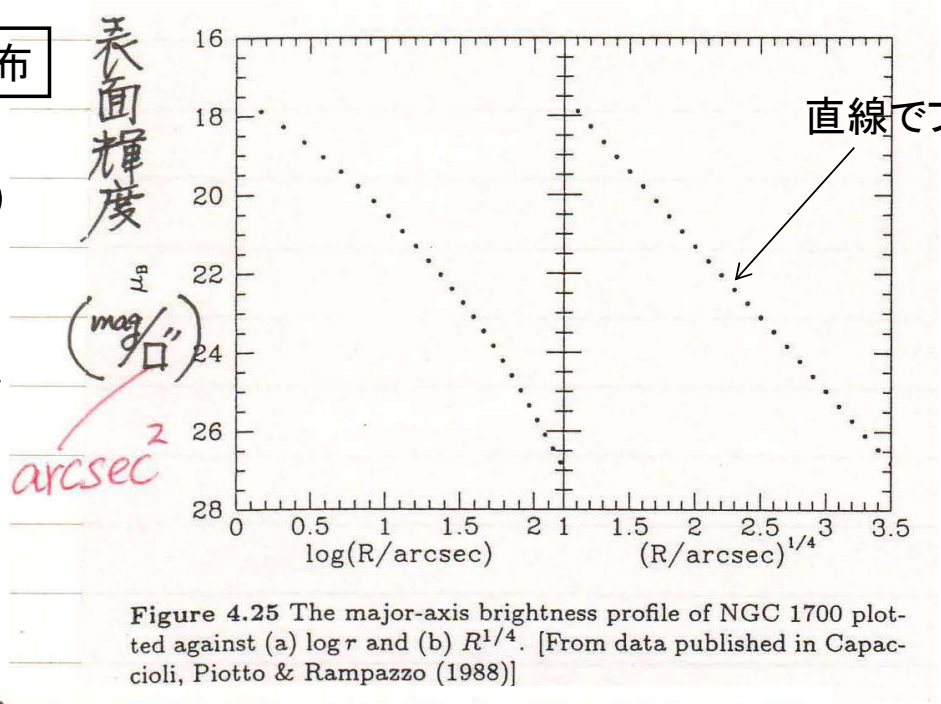

直線でフィットできる

$R^{1/4}$-law

Figure 4.25 The major-axis brightness profile of NGC 1700 plotted against (a) $\log r$ and (b) $R^{1/4}$. [From data published in Capaccioli, Piotto & Rampazzo (1988)]

楕円銀河における内部運動と光度の関係

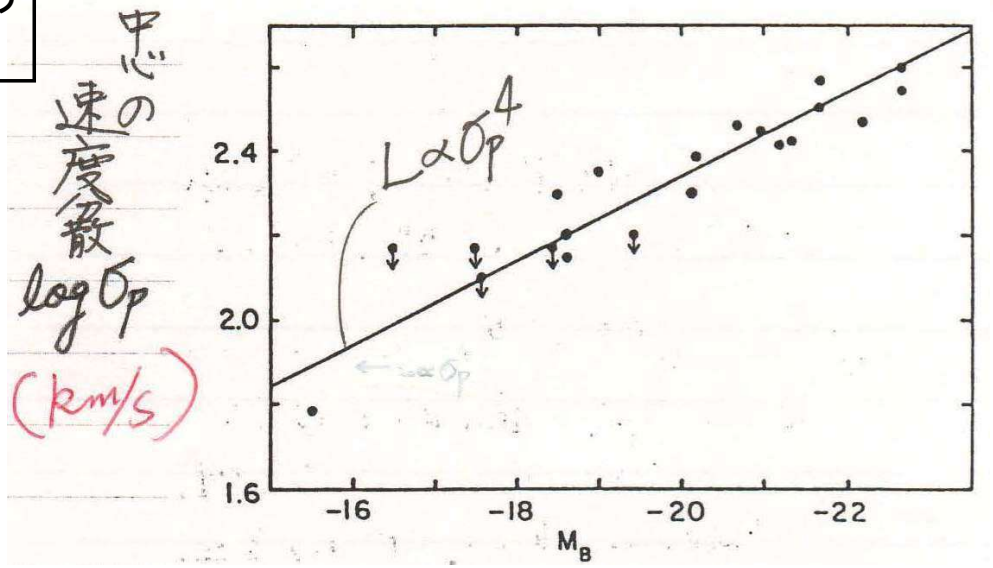

二色図
Two-color diagram

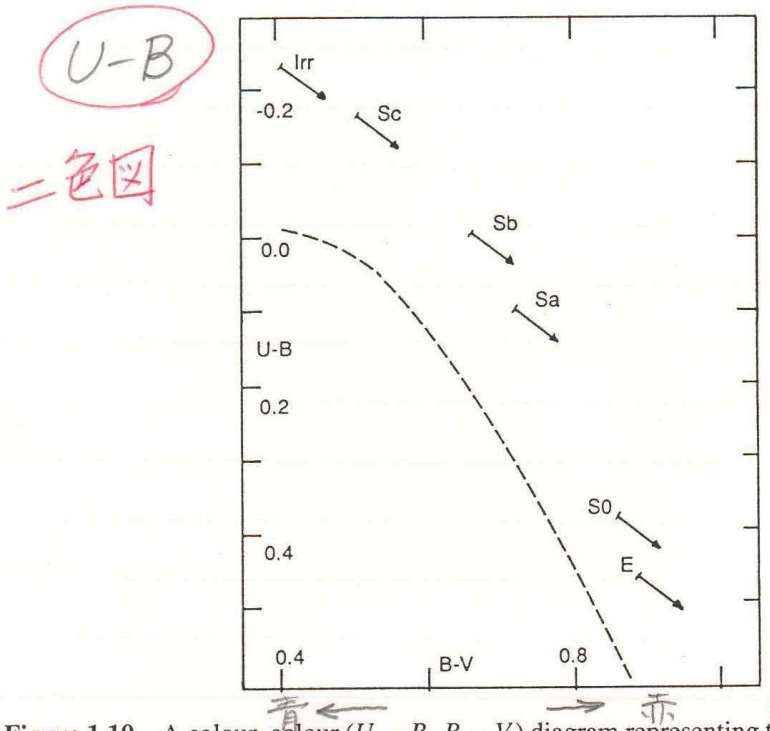

Figure 1.10 A colour–colour ($U-B$, $B-V$) diagram representing the position of normal galaxies (points) and the main sequence of stars (dashed line). The arrows indicate the effect obtained by correcting for galactic reddening, $E(B-V) = 0.06$.

色ー等級関係
Color-magnitude relation

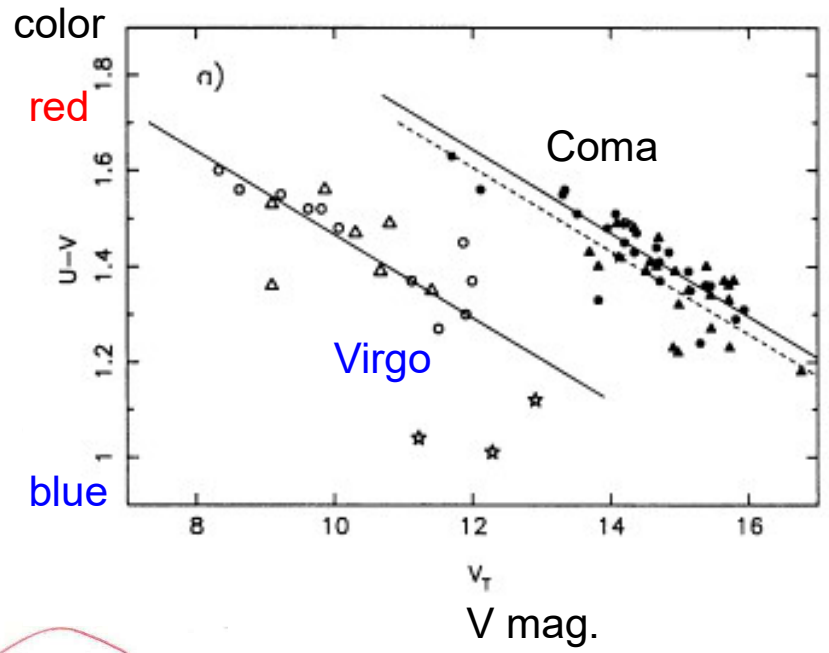

楕円銀河の中心輝度プロファイル

Faber et al. 1997

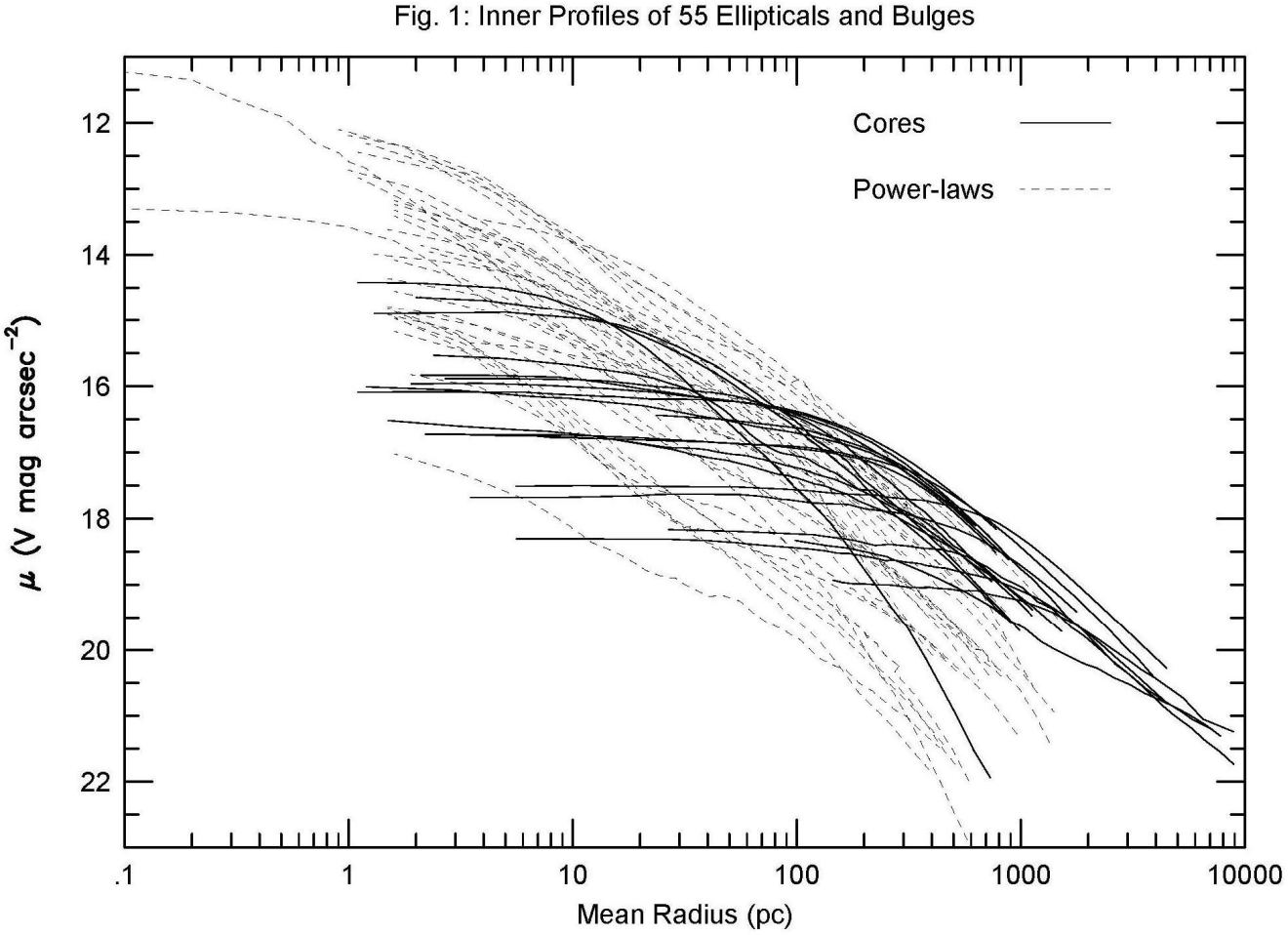

r_b : break radius, μ_b : μat break radius

Fig. 4. Central Parameters vs. Absolute Magnitude

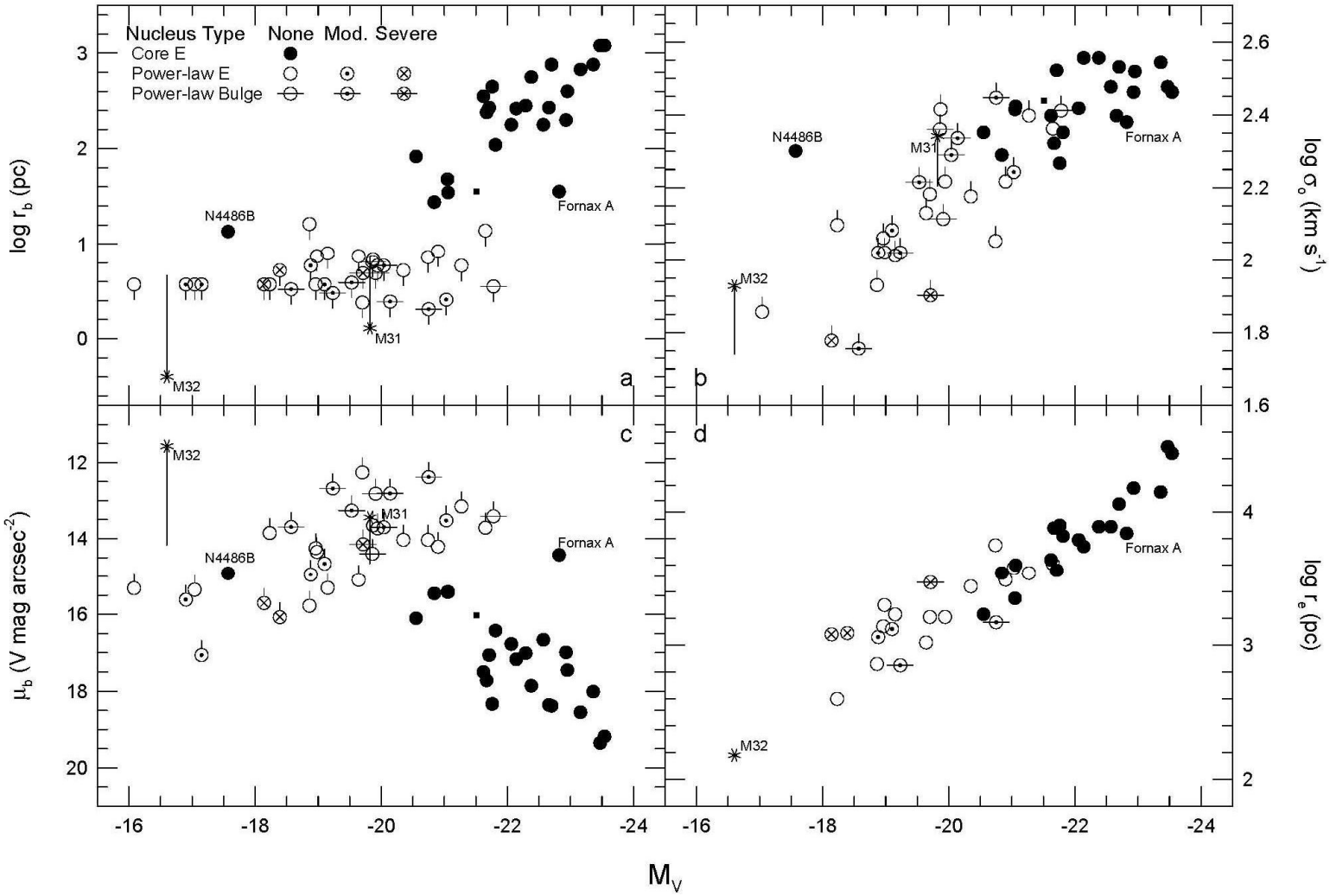

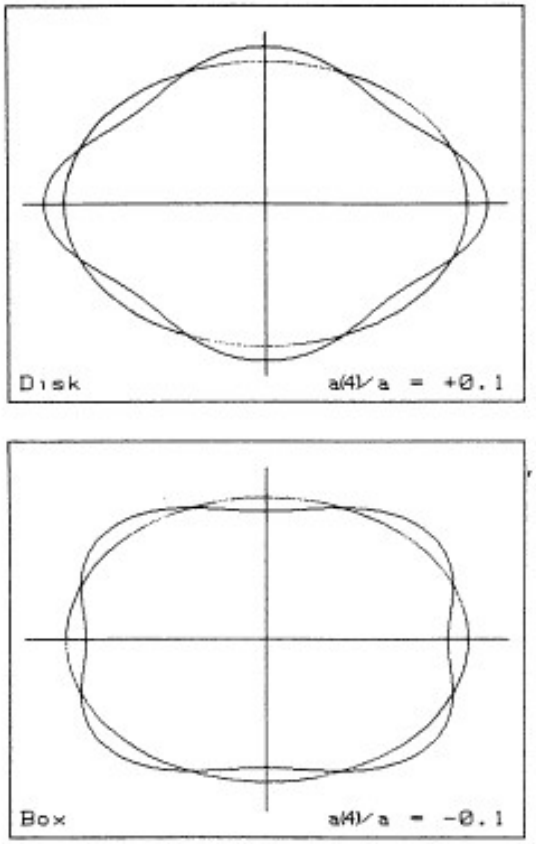

FIGURE 5. — Schematic drawing illustrating isophotes with $a(4)/a = +0.1$ and $a(4)/a = -0.1$.

Disky E

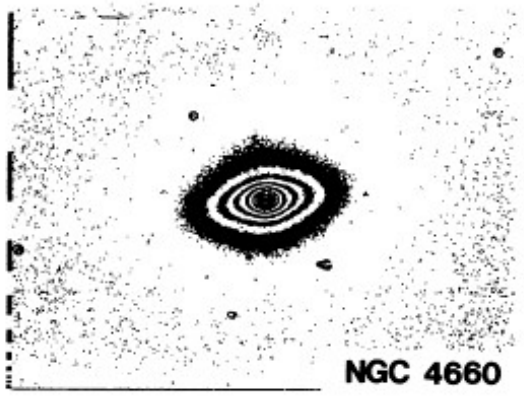

FIGURE 6. — R-image of NGC 4660, an elliptical galaxy with a disk-component in the isophotes $(a(4)/a \sim +0.03)$.

Boxy E

FIGURE 7. — R-image of NGC 5322, an elliptical galaxy with box-shaped isophotes $(a(4)/a \sim -0.01)$.

Fundamental Plane

3-d space: (σ_0, r_e, $\langle I \rangle_e$)

$$\log R_e = a \log \sigma_0 + b \log \langle I \rangle_e + \text{constant},$$

a =~ 1.5, b =~ −0.8

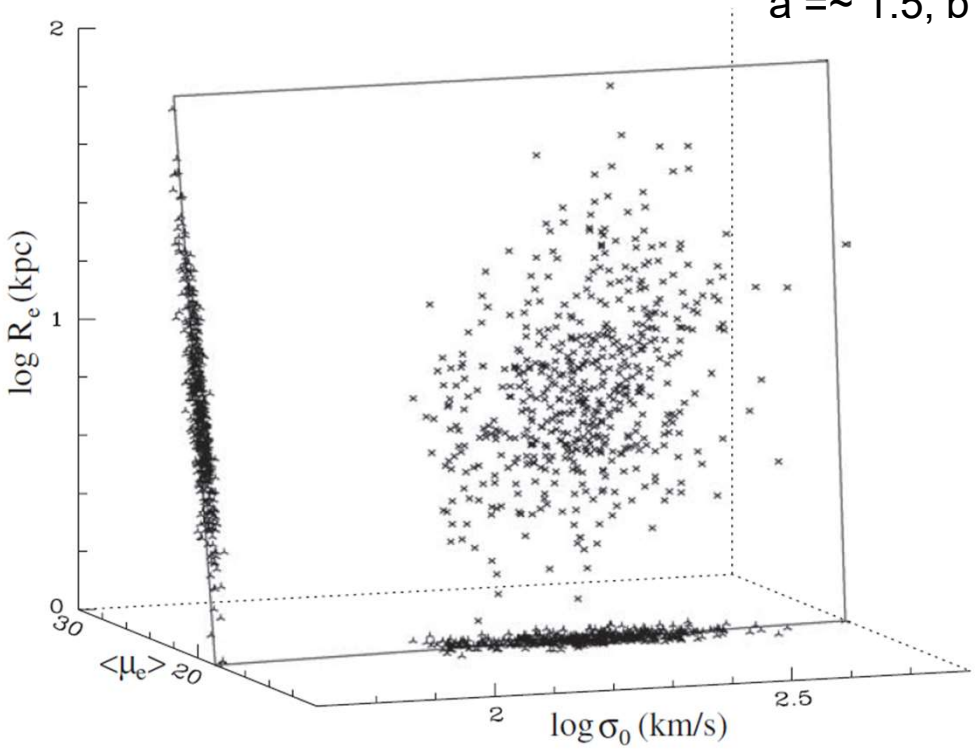

Fig. 2.18. The fundamental plane of elliptical galaxies in the $\log R_e$-$\log \sigma_0$-$\langle \mu \rangle_e$ space (σ_0 is the central velocity dispersion, and $\langle \mu \rangle_e$ is the mean surface brightness within R_e expressed in magnitudes per square arcsecond). [Plot kindly provided by R. Saglia, based on data published in Saglia et al. (1997) and Wegner et al. (1999)]

矮小銀河、楕円銀河の輝度分布

$$I(r) \propto \exp\left(-r^{n}\right)$$

I(r)

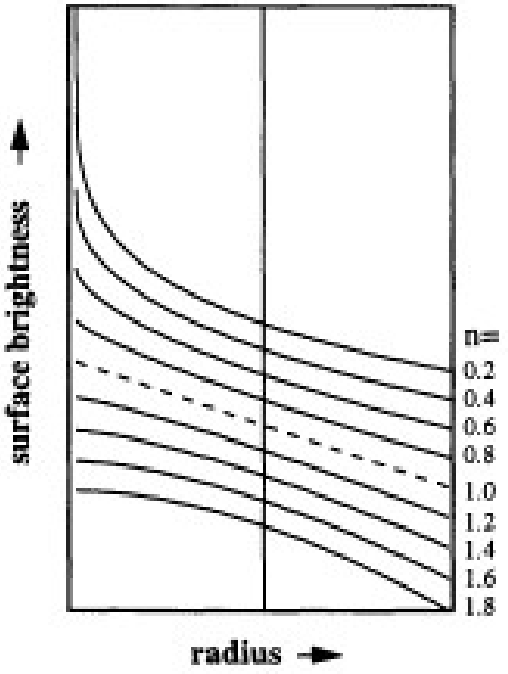

r

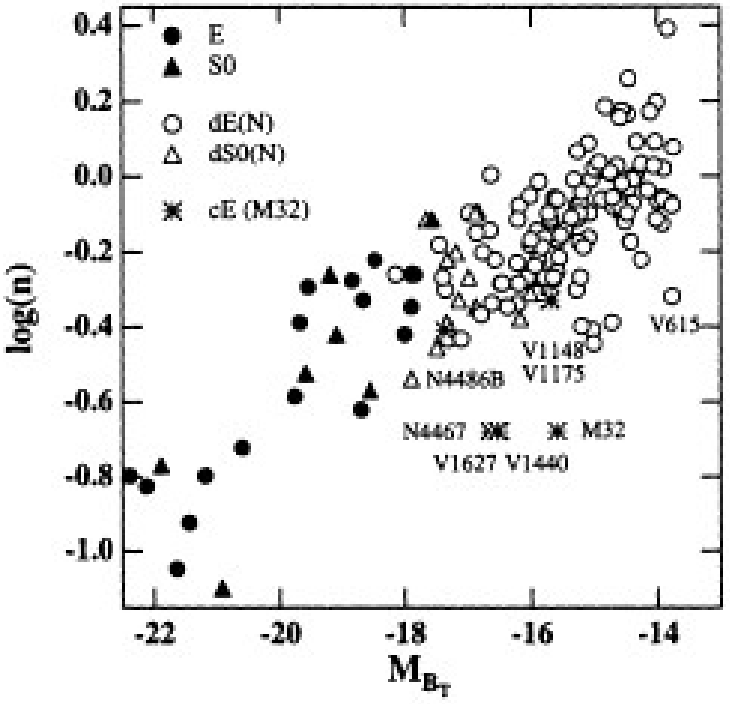

Jerjen & Binggeli 1997
In ASP conf, vol. 116

Scaling relations for spheroidal systems

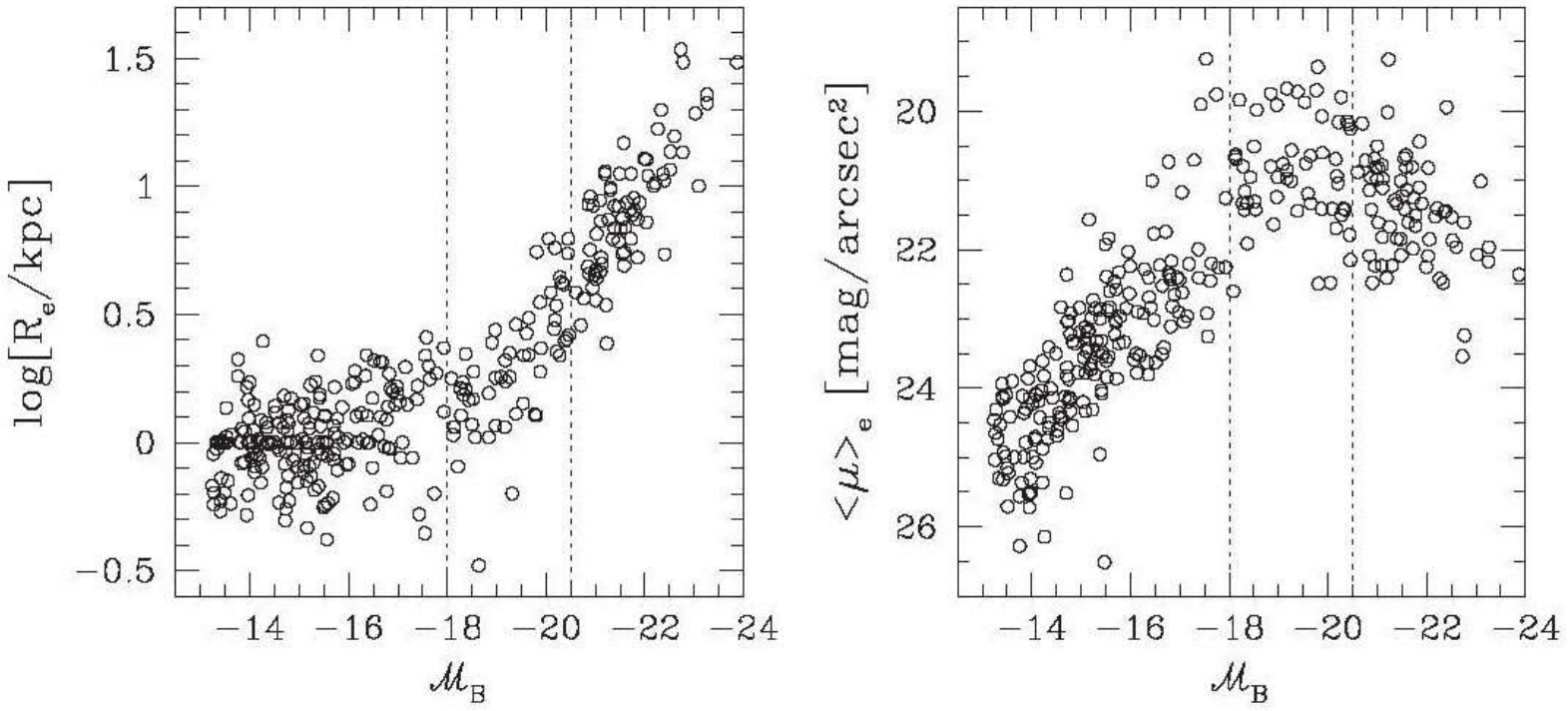

Dwarf galaxies

dwarf spheroidal galaxies
（dSphs 矮小楕円体銀河）

Leo I

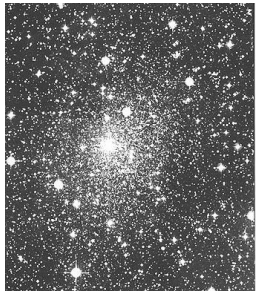

Carina

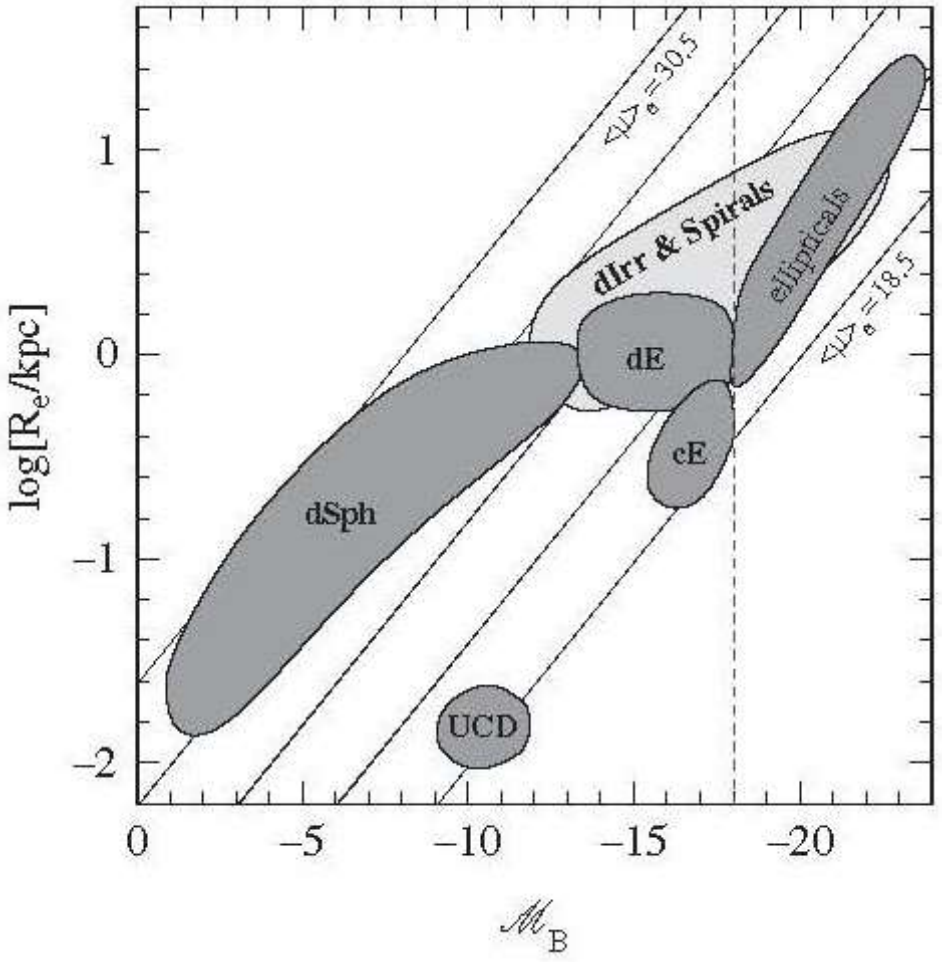

銀河団

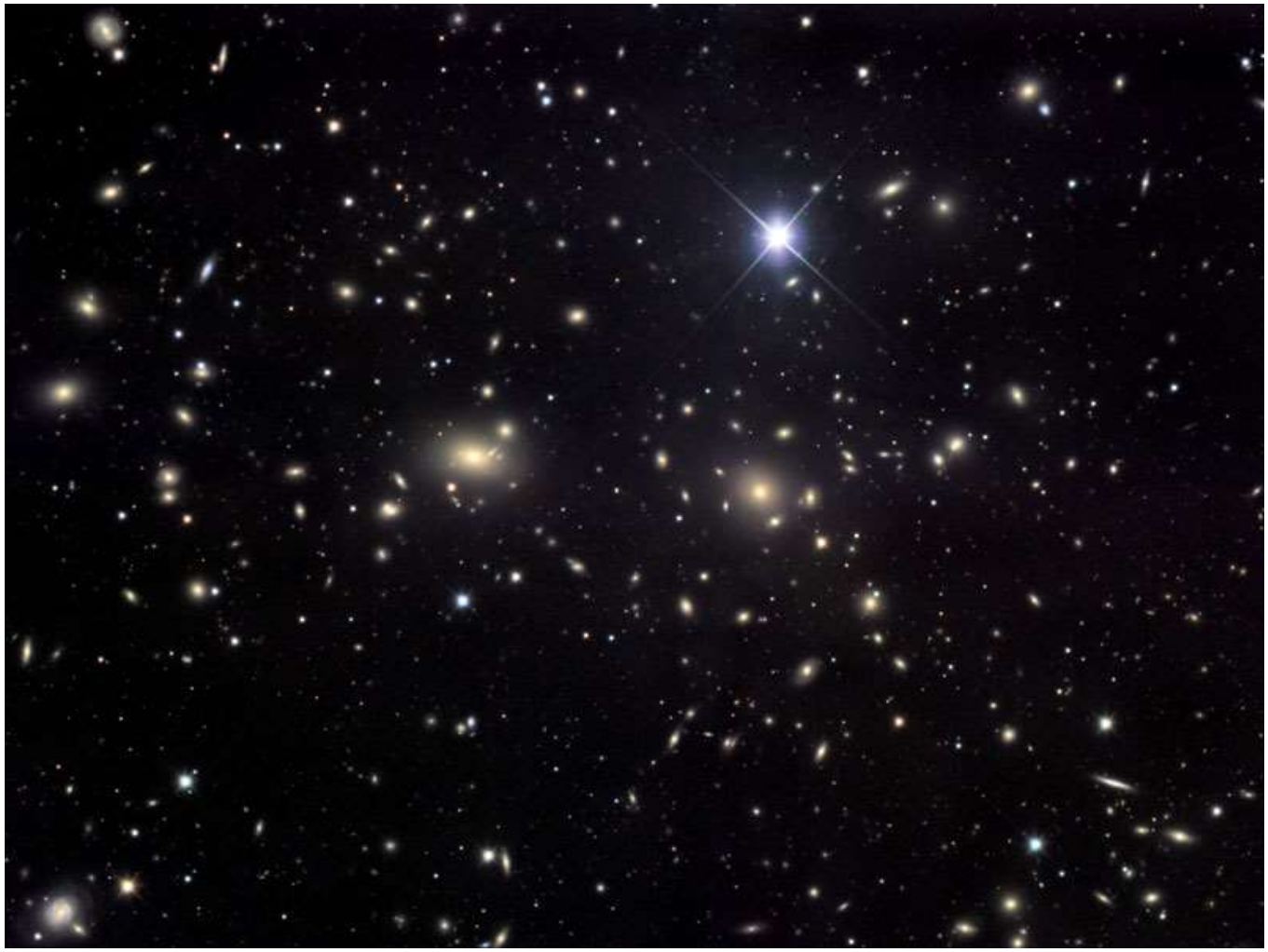

かみのけ座銀河団 Coma cluster

Morphology-density relation

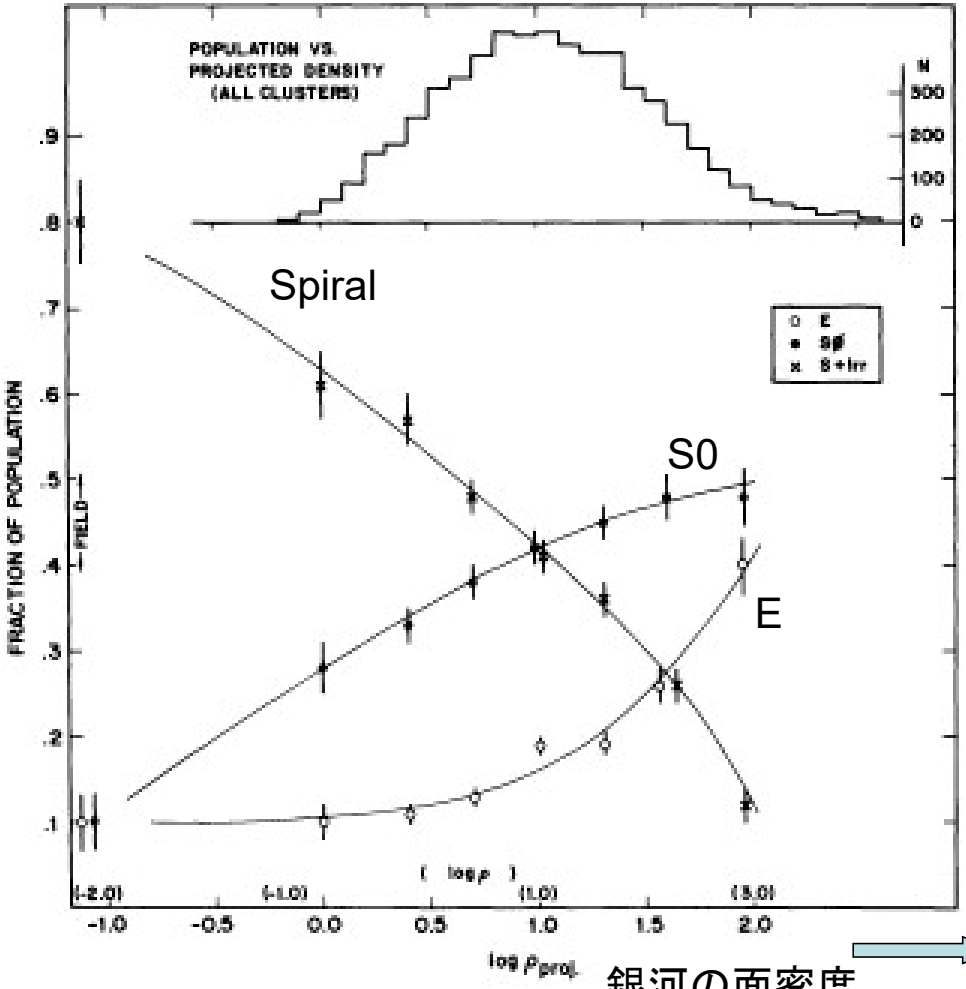

銀河形態の割合

銀河の面密度

銀河団中心

Dressler et al. 1980

Milky Way & Galactic satellites

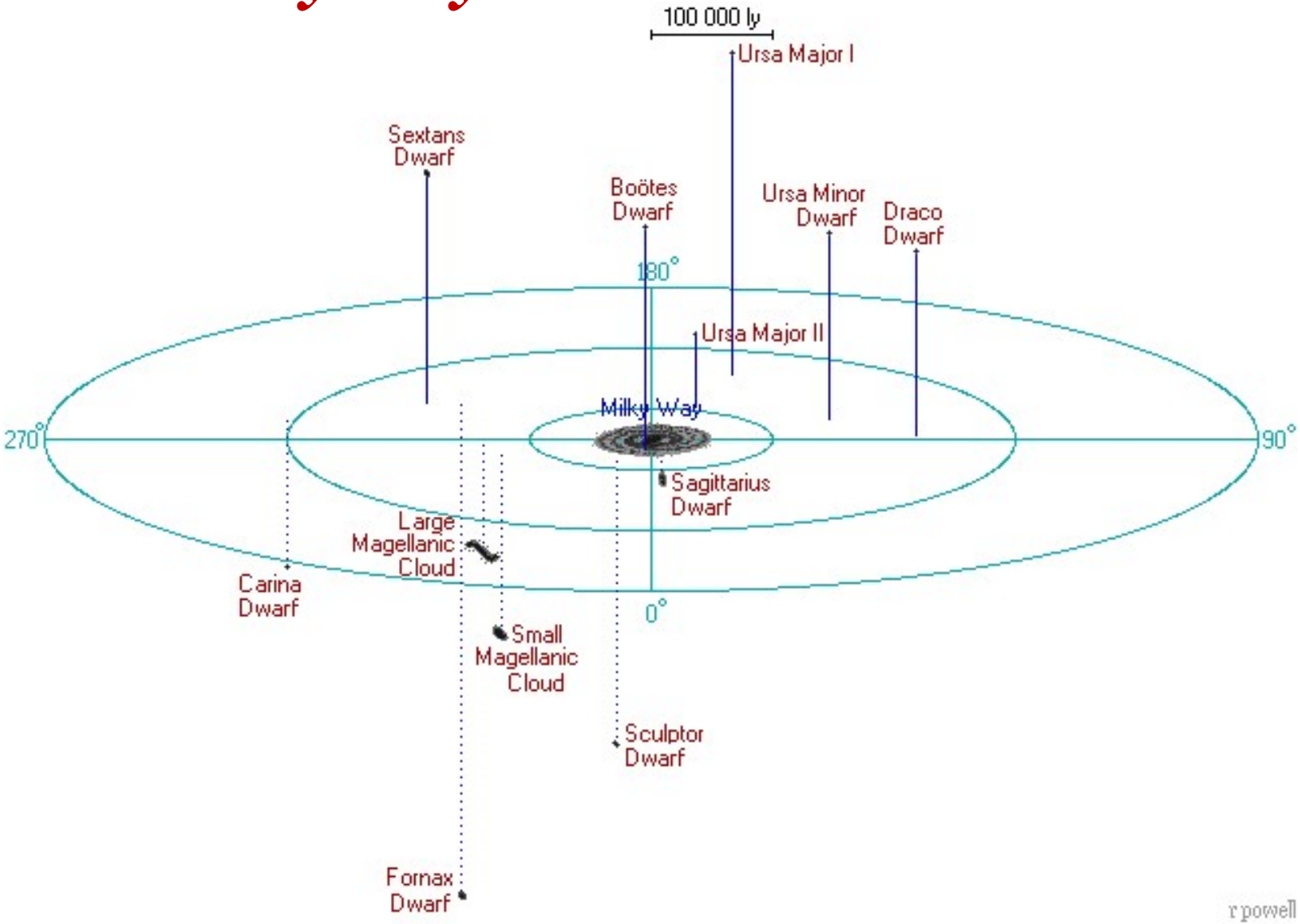

r powell

Local Group

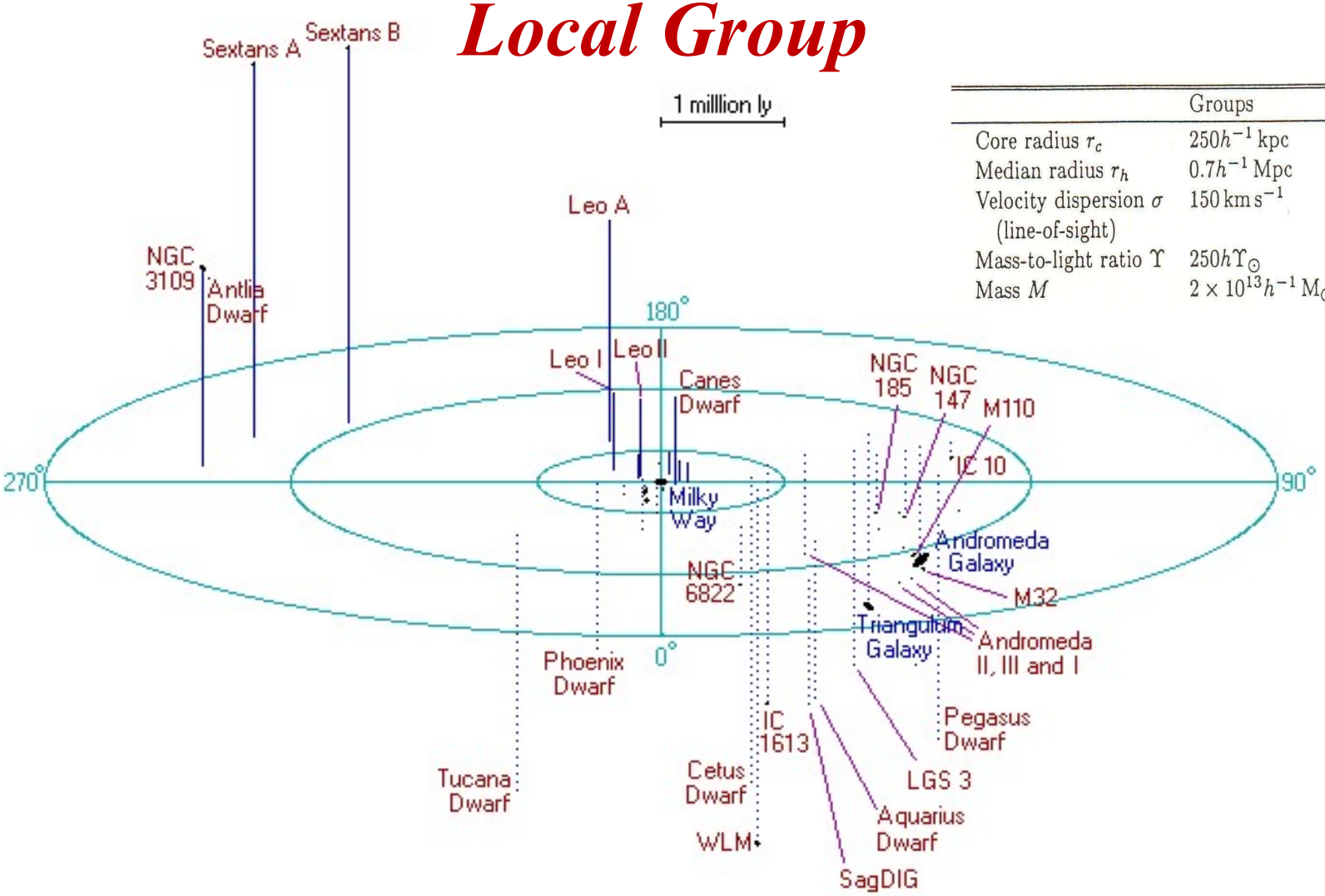

	Groups	Clusters
Core radius r_c	$250h^{-1}$ kpc	$250h^{-1}$ kpc
Median radius r_h	$0.7h^{-1}$ Mpc	$3h^{-1}$ Mpc
Velocity dispersion σ (line-of-sight)	$150\,\mathrm{km\,s^{-1}}$	$800\,\mathrm{km\,s^{-1}}$
Mass-to-light ratio Υ	$250h\Upsilon_\odot$	$250h\Upsilon_\odot$
Mass M	$2 \times 10^{13}h^{-1}\,M_\odot$	$10^{15}h^{-1}\,M_\odot$

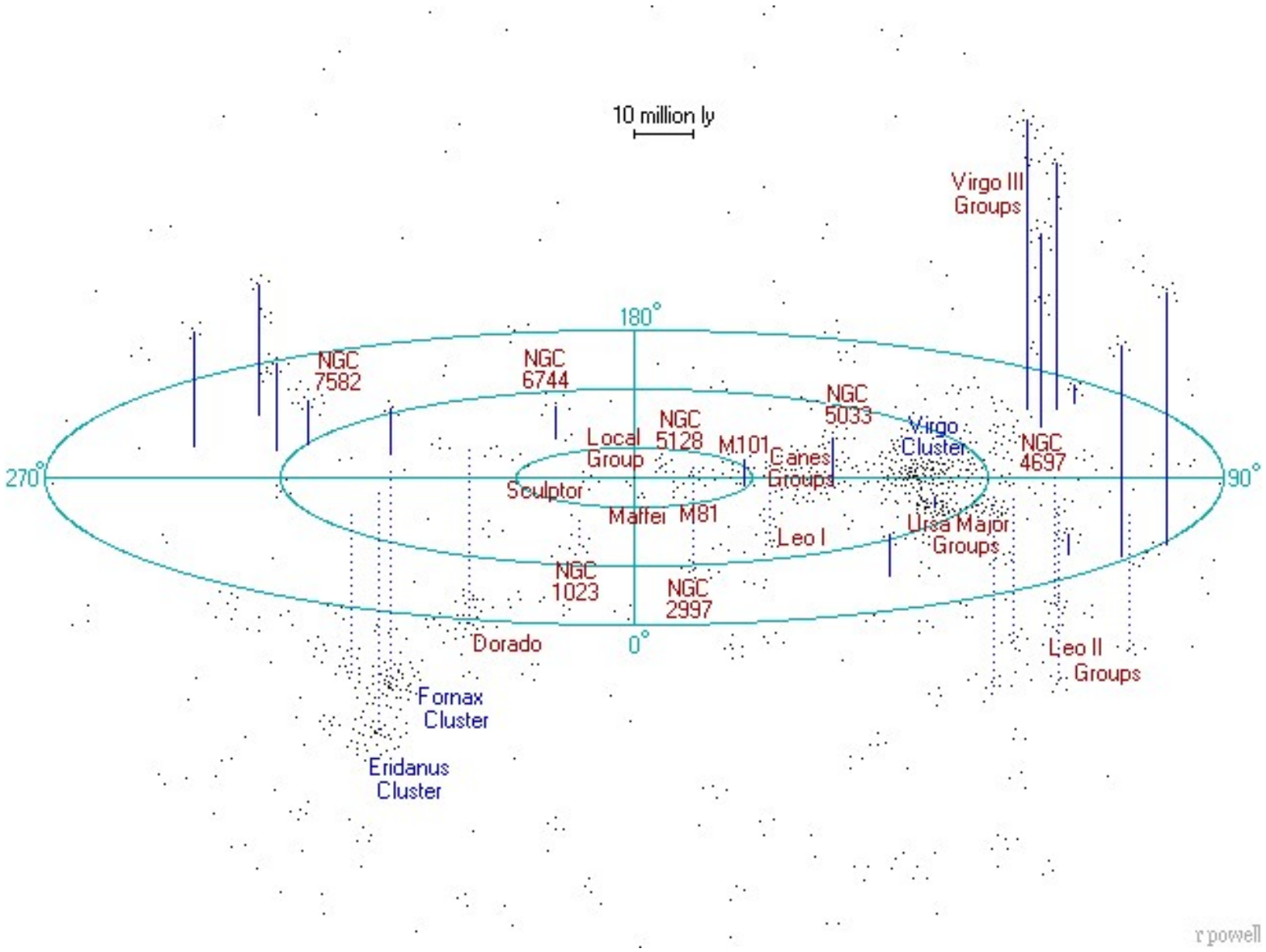
10 million ly
Virgo III
Groups
180°
NGC
7582
NGC
6744
NGC
5033
NGC
5128
Local
Group
M101
Virgo
Cluster
NGC
4697
270°
Canes
Groups
90°
Sculptor
Maffei
M81
Leo I
Ursa Major
Groups
NGC
1023
NGC
2997
Dorado
0°
Leo II
Groups
Fornax
Cluster
Eridanus
Cluster
r powell

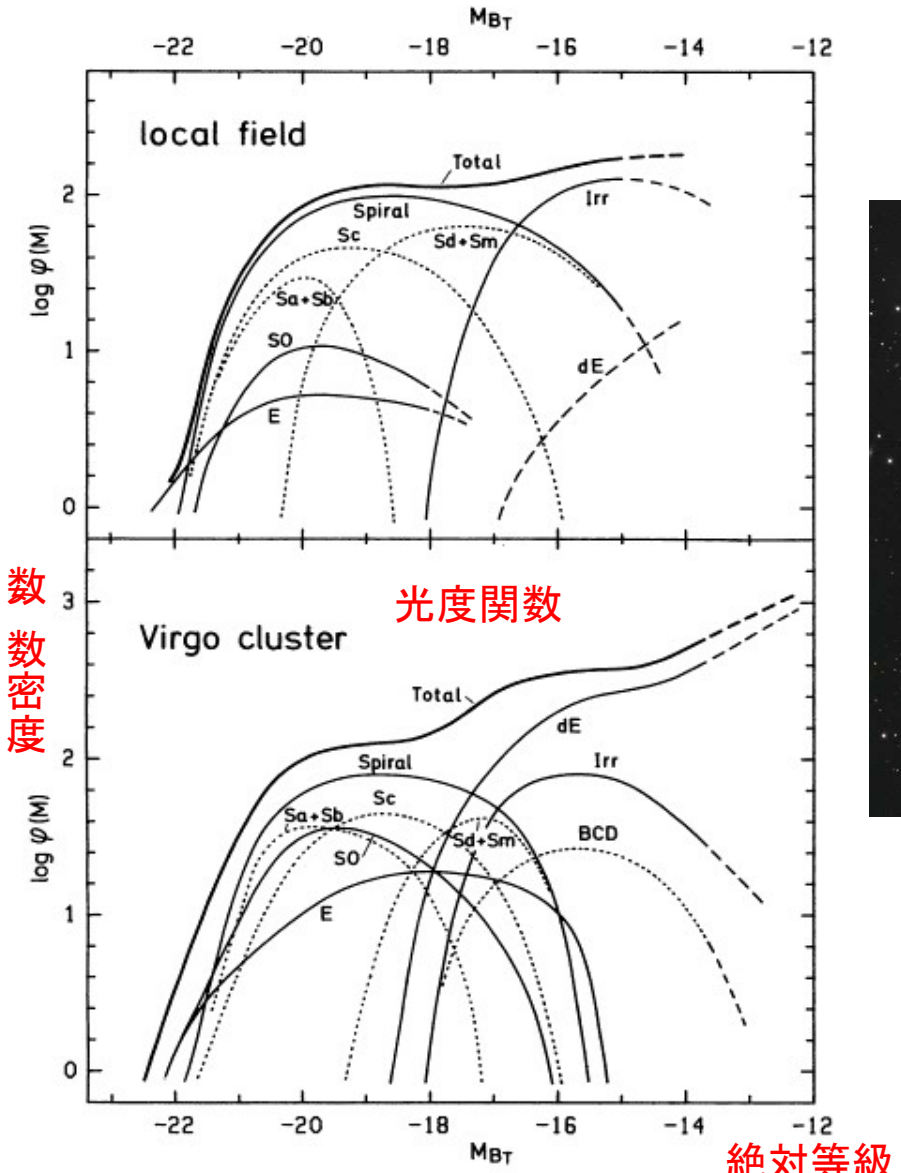

数密度

光度関数

絶対等級

Binggeli et a. 1988

おとめ座銀河団
Virgo cluster

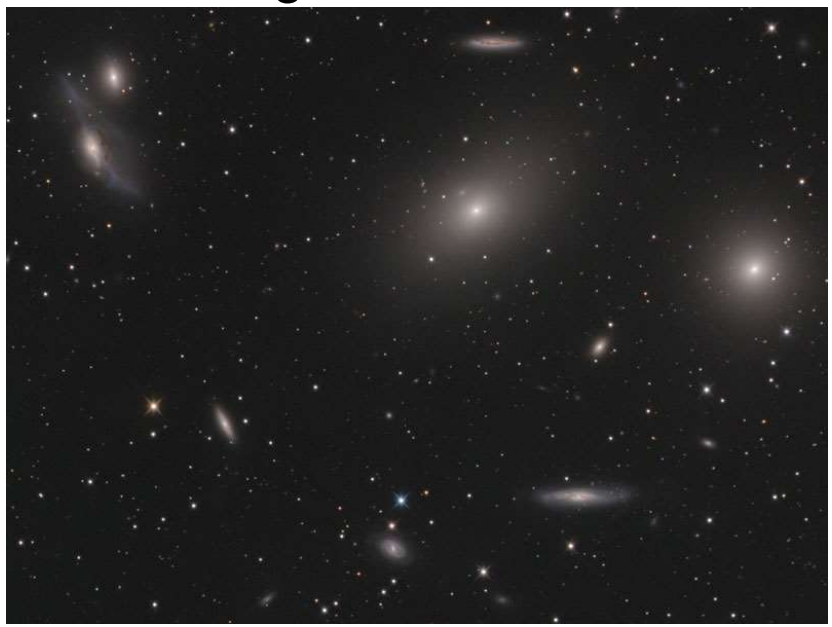

Schechter form

$$\Phi(L)dL = \Phi^* \left(\frac{L}{L^*}\right)^{\alpha} exp\left(-\frac{L}{L^*}\right) dL$$

$$L^* \sim 10^{10} L_{\odot}$$

$$\Phi^* \sim 10^{-2} Mpc^{-3}$$

$$\alpha \sim -1.0$$

CfA Survey

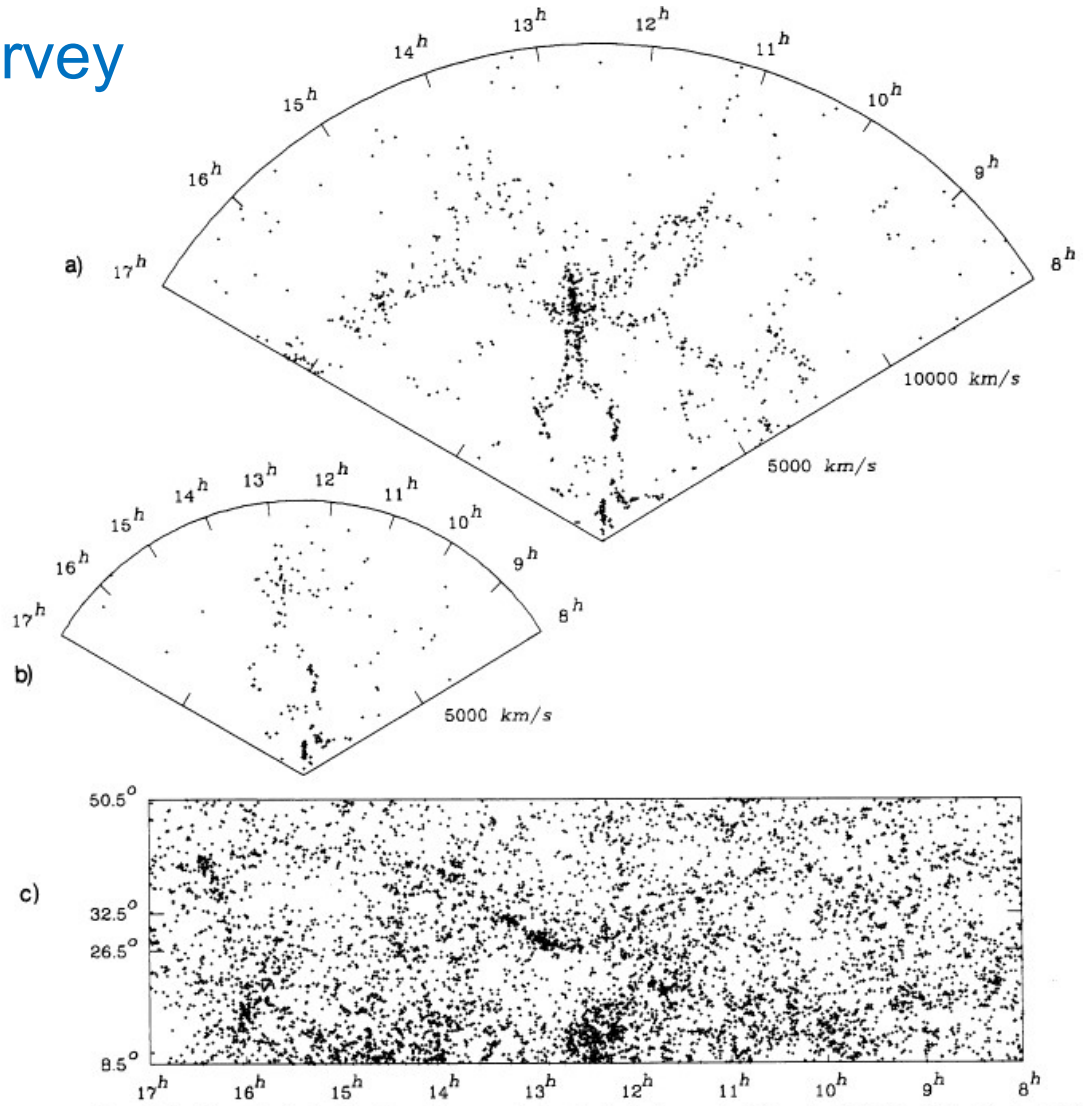

FIG. 1.—(*a*) Map of the observed velocity plotted vs. right ascension in the declination wedge $26°5 \leq \delta \leq 32°5$. The 1061 objects plotted have $m_B \leq 15.5$ and $V \leq 15{,}000$ km s^{-1}. (*b*) Same as Fig. 1*a* for $m_B \leq 14.5$ and $V \leq 10{,}000$ km s^{-1}. The plot contains 182 galaxies. (*c*) Projected map of the 7031 objects with $m_B \leq 15.5$, listed by Zwicky *et al.* in the region bounded by $8^h \leq \alpha \leq 17^h$ and $8°5 \leq \delta \leq 50°5$.

Las Campanas Redshift Survey

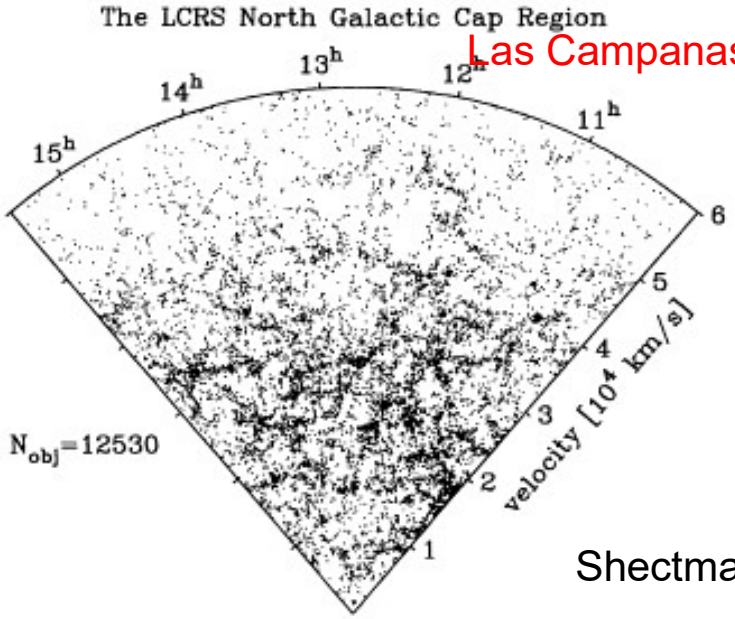

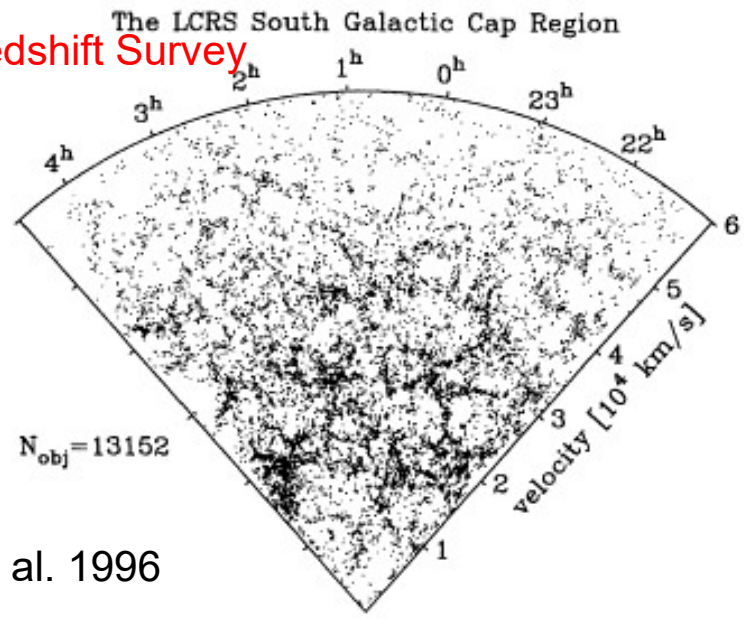

Shectman et al. 1996

数密度

(1/Mpc^3)

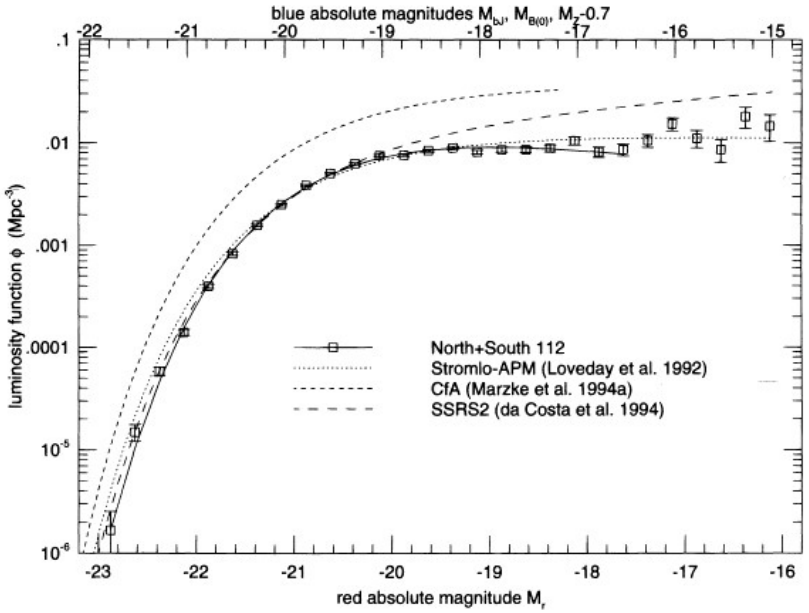

Lin et al. 1996

絶対等級

Galaxies at high redshifts

Lyman Break Galaxies (LBG)

Lyman limit: 912 A

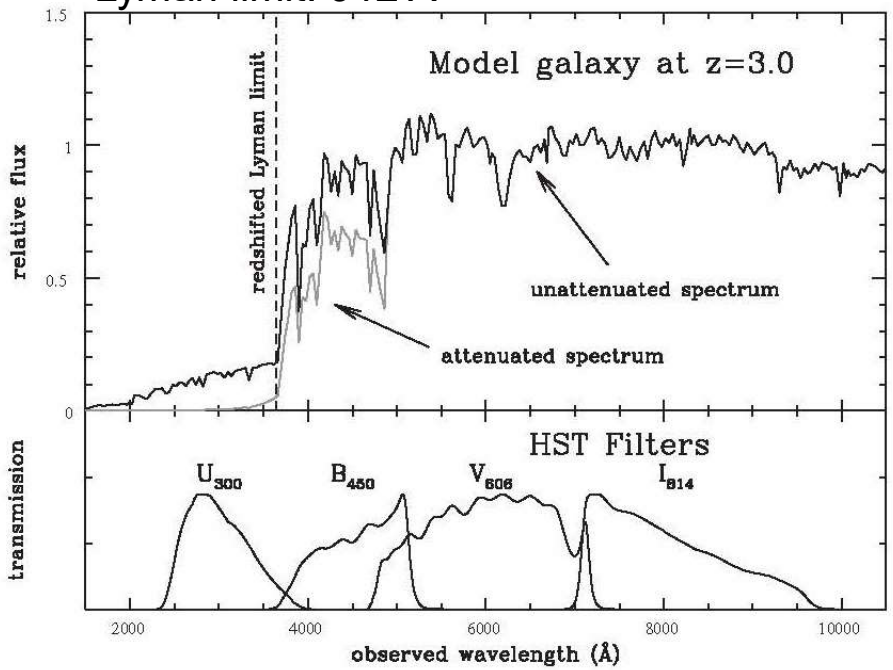

Lyman alpha Emitters (LAE)

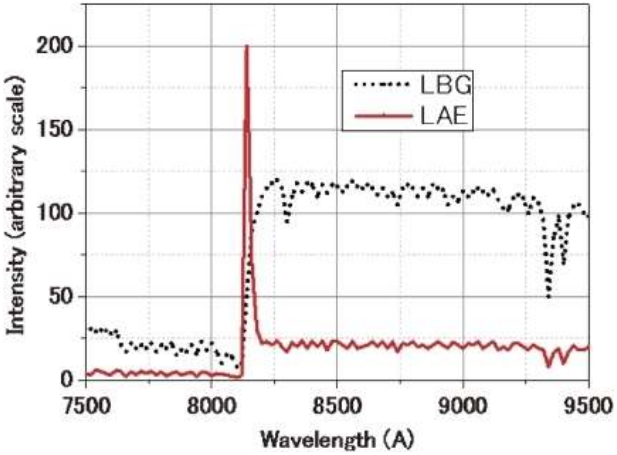

Lyman alpha Blob (LAB)

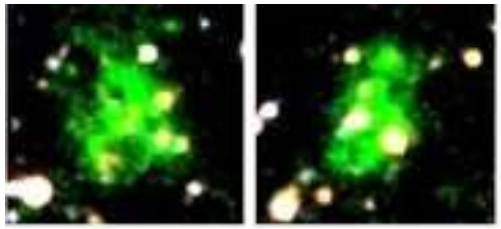

様々な観測から求められた宇宙における星形成史
Madau & Dickinson (2014)